Center for Environmentally Sustainable Transportation in Cold Climates

Prediction of Thermal Behavior of Pervious Concrete Pavements in Winter

Authors:
Zhao Chen, Benjamin Nantasai, Somayeh Nassiri, Liv Haselbach
Department of Civil and Environmental Engineering
Washington State University

Date: May 15 2017

Prepared by:
Center for Environmentally Sustainable
Transportation in Cold Climates
University of Alaska Fairbanks
P.O. Box 755900
Fairbanks, AK 99775

U.S. Department of Transportation
1200 New Jersey Avenue, SE
Washington, DC 20590

INE/AUTC 17.12

REPORT DOCUMENTATION PAGE

Form approved OMB No.

1. AGENCY USE ONLY (LEAVE BLANK)	2. REPORT DATE	3. REPORT TYPE AND DATES COVERED
	May 15, 2017	Final Report: May 15, 2017

4. TITLE AND SUBTITLE
Prediction of Thermal Behavior of Pervious Concrete Pavements in Winter

5. FUNDING NUMBERS

6. AUTHOR(S)
Zhao Chen, PhD student; Benjamin Nantasai, MS student; Somayeh Nassiri, Assistant Professor; Liv Haselbach, Professor

7. PERFORMING ORGANIZATION NAME(S) AND ADDRESS(ES)
Center for Environmentally Sustainable Transportation in Cold Climates
University of Alaska Fairbanks
Duckering Building Room 245
P.O. Box 755900
Fairbanks, AK 99775-5900

8. PERFORMING ORGANIZATION REPORT NUMBER

9. SPONSORING/MONITORING AGENCY NAME(S) AND ADDRESS(ES)
U.S. Department of Transportation
1200 New Jersey Avenue, SE
Washington, DC 20590

10. SPONSORING/MONITORING AGENCY REPORT NUMBER

11. SUPPLENMENTARY NOTES

12a. DISTRIBUTION / AVAILABILITY STATEMENT
No restrictions

12b. DISTRIBUTION CODE

13. ABSTRACT (Maximum 200 words)

Because application of pervious concrete pavement (PCPs) has extended to cold-climate regions of the United States, the safety and mobility of PCP installations during the winter season need to be maintained. Timely application of salt, anti-icing, and deicing agents for ice/snow control is most effective in providing sufficient surface friction when done at a suitable pavement surface temperature. The aim of this project was to determine the thermal properties of PCP during the winter season, and to develop a theoretical model to predict PCP surface temperature. The project included a laboratory and a field component. In the laboratory, thermal conductivity of pervious concrete was determined. A linear relationship was established between thermal conductivity and porosity for pervious concrete specimens. In the field, the pavement temperature in a PCP sidewalk installation at Washington State University was monitored via in-pavement instrumentation. Based on the field data, the Enhanced Integrated Climatic Model (EICM) was developed and validated for the site, using PCP thermal properties and local climatic data. The EICM-predicted PCP surface temperature during the winter season agreed well with the field temperature. Overall, the predicted number of days that the pavement surface fell below 32°F agreed well with the number based on field data for 85% of the days. Therefore, the developed model is useful in identifying those days to apply deicer agents. Finally, a regression model using climatic indices was developed for PCP surface temperature prediction in the absence of a more advanced temperature model.

14- KEYWORDS:
Concrete pavements, Deicers, Winter maintenance, Frost, Surface temperature, Heat transfer, Thermal conductivity

15. NUMBER OF PAGES
74

16. PRICE CODE
N/A

17. SECURITY CLASSIFICATION OF REPORT	18. SECURITY CLASSIFICATION OF THIS PAGE	19. SECURITY CLASSIFICATION OF ABSTRACT	20. LIMITATION OF ABSTRACT
Unclassified	Unclassified	Unclassified	N/A

Disclaimer

This document is disseminated under the sponsorship of the U. S. Department of Transportation in the interest of information exchange. The U.S. Government assumes no liability for use of the information contained in this document. The U.S. Government does not endorse products or manufacturers. Trademarks or manufacturers' names appear in this report only because they are considered essential to the objective of the document. Opinions and conclusions expressed or implied in the report are those of the author(s). They are not necessarily those of the funding agencies.

METRIC (SI*) CONVERSION FACTORS

APPROXIMATE CONVERSIONS TO SI UNITS

Symbol	When You Know	Multiply By	To Find	Symbol
		LENGTH		
in	inches	25.4		mm
ft	feet	0.3048		m
yd	yards	0.914		m
mi	Miles (statute)	1.61		km
		AREA		
in^2	square inches	645.2	millimeters squared	cm^2
ft^2	square feet	0.0929	meters squared	m^2
yd^2	square yards	0.836	meters squared	m^2
mi^2	square miles	2.59	kilometers squared	km^2
ac	acres	0.4046	hectares	ha
		MASS (weight)		
oz	Ounces (avdp)	28.35	grams	g
lb	Pounds (avdp)	0.454	kilograms	kg
T	Short tons (2000 lb)	0.907	megagrams	mg
		VOLUME		
fl oz	fluid ounces (US)	29.57	milliliters	mL
gal	Gallons (liq)	3.785	liters	liters
ft^3	cubic feet	0.0283	meters cubed	m^3
yd^3	cubic yards	0.765	meters cubed	m^3
		TEMPERATURE (exact)		
ºF	Fahrenheit temperature	5/9 (ºF-32)	Celsius temperature	ºC
		ILLUMINATION		
fc	Foot-candles	10.76	lux	lx
fl	foot-lamberts	3.426	candela/m^2	cd/cm^2
		FORCE and PRESSURE or STRESS		
lbf	pound-force	4.45	newtons	N
psi	pound-force per square inch	6.89	kilopascals	kPa

Note: Volumes greater than 1000 L shall be shown in m^3

These factors conform to the requirement of FHWA Order 5190.1A *SI is the symbol for the International System of Measurements

APPROXIMATE CONVERSIONS FROM SI UNITS

Symbol	When You Know	Multiply By	To Find	Symbol
		LENGTH		
mm	millimeters	0.039	inches	in
m	meters	3.28	feet	ft
m	meters	1.09	yards	yd
km	kilometers	0.621	Miles (statute)	mi
		AREA		
mm^2	millimeters squared	0.0016	square inches	in^2
m^2	meters squared	10.764	square feet	ft^2
km^2	kilometers squared	0.39	square miles	mi^2
ha	hectares (10,000 m^2)	2.471	acres	ac
		MASS (weight)		
g	grams	0.0353	Ounces (avdp)	oz
kg	kilograms	2.205	Pounds (avdp)	lb
mg	megagrams (1000 kg)	1.103	short tons	T
		VOLUME		
mL	milliliters	0.034	fluid ounces (US)	fl oz
liters	liters	0.264	Gallons (liq)	gal
m^3	meters cubed	35.315	cubic feet	ft^3
m^3	meters cubed	1.308	cubic yards	yd^3
		TEMPERATURE (exact)		
ºC	Celsius temperature	9/5 ºC+32	Fahrenheit temperature	ºF
		ILLUMINATION		
lx	lux	0.0929	foot-candles	fc
cd/cm^2	candela/m^2	0.2919	foot-lamberts	fl
		FORCE and PRESSURE or STRESS		
N	newtons	0.225	pound-force	lbf
kPa	kilopascals	0.145	pound-force per square inch	psi

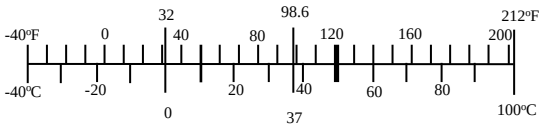

Acknowledgment

The authors acknowledge funding support for the project from the Center for Environmentally Sustainable Transportation in Cold Climates. Washington State University's Facility Services is also acknowledged for providing matching funds for the project and for its cooperation during installation of the pervious concrete pavement on Washington State University's campus.

Table of Contents

List of Figures

List of Tables

Executive Summary

The safety and mobility of pervious concrete pavement (PCP) installations during the winter season need to be maintained since the application of PCPs has extended to cold-climate regions of the United States. Timely application of salt, anti-icing, and deicing agents for ice/snow control is most effective in providing sufficient surface friction when done at a suitable pavement surface temperature. Thus, the ability to predict PCP surface temperature during winter is beneficial to ice/snow control of PCPs. The aim of this project was to determine the thermal properties of PCP during the winter season and to develop a theoretical model to predict PCP surface temperature to facilitate PCP winter maintenance policies.

The project included a laboratory and a field component. In the laboratory, thermal conductivity (k) of pervious concrete (PC) in wet and dry conditions was determined by two methods: 1) the heat flow meter and 2) the sensor probe. A linear relationship was established between thermal conductivity and porosity for PC specimens. In addition, to overcome the fact that laboratory characterization of k for different PC mixtures is not always feasible, a geometric parallel model using the percent volumetric fractions and k of the three main components: aggregate, concrete paste, and air void was introduced and applied. This model agreed well with the measured k of the dry PC samples, while the prediction for wet samples was not as good as dry samples since water wets the air pockets and fills the various pores of the aggregate and paste in the PC.

In the field, the pavement temperature in a PCP sidewalk installation at Washington State University was monitored via in-pavement instrumentation. Based on the field data, the Enhanced Integrated Climatic Model (EICM) was developed and validated for the site, using PCP thermal properties and local climatic data, including ambient temperature, wind speed,

radiation of the sky, relative humidity, and precipitation. Overall, the EICM-predicted number of days that the pavement surface fell below 32°F agreed well with the number based on field data for 85% of the days. Therefore, the developed model is useful in identifying those days to apply deicer agents. Finally, in the absence of a more advanced temperature prediction model, a regression model using climatic indices (temperature, relative humidity, wind speed, and solar radiation) was developed for PCP surface temperature prediction. The *p*-value of the regression is less than 0.001 at 98% confidence interval with a mean standard error of 0.2°F and R^2 of 0.98. This regression model can be used as an estimation of temperature prediction at the PCP surface.

More research is needed for PC thermal properties, including more mixture design and aggregate types at different porosities to add to the database developed in this study and develop a comprehensive PC property model ultimately. Research on thermal properties of the base layer and thermal conduction between the PCP and base layer may improve the accuracy of the temperature prediction model. The regression model developed in this study need to be validated with more data and can be further expanded to include the thermophysical properties and structure characteristics of the PC pavements.

CHAPTER 1. INTRODUCTION

1.1 Research Significance

Pervious concrete pavements (PCPs) are growing in popularity, especially for municipal flatwork applications such as sidewalks and pathways, collector and local (low-traffic volume) streets, parking lots, and driveways. As PCP usage extends to cold-climate regions of the United States, the aspects of safety and mobility in PCP application during the winter season are growing in importance. There is a need for the development of proper winter maintenance practices that take into account the effect of the void structure of PCP on thermal behavior during winter. The ability to predict the surface temperature of PCP during winter benefits ice/snow control operations that are sensitive to pavement surface temperature. These operations include the application of salt, anti-icing, and deicing agents, which are most effective with timely application. In this study, steps are taken to predict the thermophysical properties of PCP both in the laboratory and in the field. A temperature model for the prediction of PCP surface temperature using local climatic indices is presented.

1.2 Objectives of the Study

The long-term objective of this research was to facilitate the development of winter maintenance policies suitable for pervious concrete installations. Specific objectives included:

1. Establishing the thermal conductivity (k) of pervious concrete (PC) as a function of volumetric air void content (porosity) under dry and wet conditions in the laboratory.

2. Using field data to develop and validate a model to predict the surface temperature of PCP during the winter season.

3. Developing a statistical relation to predict the PCP surface temperature based on major meteorological indices.

1.3 Methodology

A pervious concrete slab and cylindrical specimens were cast and air cured in the laboratory. After a 7-day air-curing period, the physical properties of PC, including infiltration, density, and hardened porosity, were determined by nondestructive tests. Next, the *k* of PC was obtained in both dry and wet conditions for slabs using two different test methodologies: heat flow and heat impulse analysis. The latter method was used on the top and bottom of twenty cylinders that were saw cut in two halves. Based on test data, linear relationships were obtained between *k* and porosity that can be used by others to estimate conductivity. A geometric parallel model was found to predict the experimentally obtained *k* for the tested specimens.

One PC sidewalk installation was constructed and instrumented at the campus of Washington State University (WSU) – Pullman in May 2015. Temperature sensors were installed in the sidewalk throughout the 6-inch-deep slab. A local weather station on campus provided the meteorological data for the site, except for solar radiation. A pyranometer sensor was installed at the project site to capture radiation from the sky, accounting for cloud-cover conditions. Data from the sensors were collected in 15-minute intervals and were stored in the datalogger starting on May 20, 2015, at 3:00 PM. Data are graphically presented in this report and evaluated based on ambient conditions over the monitoring period.

Enhanced Integrated Climatic Model (EICM) computer software was used to predict the surface temperature of PCP during the winter season, using site climatic data, including ambient temperature, wind speed, solar radiation, precipitation, and relative humidity (RH) (Larson and Dempsey 1997). Thermophysical parameters were entered in the software to closely represent the properties of the PCP sidewalk, since the EICM was originally developed for the evaluation of traditional concrete pavements and asphalt pavements. The temperature predictions were

compared with the measured temperature of PCP from the field, and statistical analysis was conducted to evaluate the level of accuracy of the temperature predictions.

1.4 Literature Review

1.4.1. Pervious Concrete Pavement

Pervious concrete is a porous-structured class of concrete that is highly permeable (typical infiltration rate is 100–2000 inches per hour) (Chopra et al. 2006). Most PC mixtures contain coarse aggregate, water, portland cement paste, and a small amount of fine aggregate or none at all. The small amount of fine aggregate, if added, is to improve the PC's strength and durability (Delatte et al. 2007). Pervious concrete mixtures typically have low water-to-cement ratios (w/cm) ranging from 0.27–0.4 compared with the w/cm of typical portland cement concrete (PCC) used for highway paving. Another characteristic of PCP is the low slump and (therefore) workability, which is generally less than ¾ inch (Kevern et al. 2009 a). Compaction and finishing processes have a great effect on the durability and performance of PCPs. Surface raveling can be prevented by proper finishing, assuring a uniform and level surface. Furthermore, PCP is more durable when cured under plastic cover for a minimum of 7 days (Kevern and Schaefer 2013). The hardened porosity of PCP ranges from 15–35% (most frequently around 20%) (Obla and Sabnis 2009), allowing PCP to drain runoff through the pavement structure and, in some applications, naturally recharge the groundwater table. Thus, PCP is considered an environmentally friendly pavement and an effective tool for stormwater management (Kosmatka et al. 2002, Haselbach et al. 2011). Pervious concrete pavement can qualify for Leadership in Energy and Environmental Design (LEED) Green Building Rating System credits, when used in building site designs: sidewalks, parking lots, streets, and plaza areas (Ashley 2008). The free-

draining structure reduces ponding on the pavement surface, thus reducing the chances of hydroplaning (Kevern and Schaefer 2013).

1.4.2. Maintenance Practices

Regular maintenance operations are required for PCP to avoid clogging over time from an accumulation of fine materials and debris (Haselbach et al. 2011). Fine sediments can cause clogging on the PCP surface, which can subsequently reduce permeability (Haselbach et al. 2011). Routine maintenance of vacuuming or power washing has been found to improve permeability by 80–90% of the original permeability (Tong 2011). Frequent maintenance activities can be reduced by providing an erosion control fence at the site or by providing established vegetation in the surrounding areas (Shu et al. 2011).

Regarding winter maintenance operations, deicing salt or chemicals are often applied to the pavement surface to lower the freezing point of moisture that collects on the surface. The goal is to improve the safety of pedestrians and drivers, while reducing the overall costs of winter road maintenance operations during snow/ice conditions. In general, chemical interactions between deicers and cement hydration products over time may result in deterioration of the concrete. Best deicing practices suggest an adequate amount of deicer applications using less than 4% solution by weight to decrease the potential for scaling of the pavement surfaces (PCA 2015). The benefit of reduced deicer chemical usage leads to the reduction in contamination of natural resources (EPA 2002). Research on the extent of damage in PCP in the presence of deicers is needed (Schaefer et al. 2010).

This research study attempts to predict the temperature of PCP during the winter season to set the groundwork for developing standardized winter maintenance operations for PCP. If best timing for deicer applications can be predicted, usage of deicers can be minimized, which

can result in longer service life of PCP. The following sections discuss literature regarding thermal properties and temperature of PCP as well as heat transfer in pavement systems.

1.4.3. Temperature Measurements in PCP

The heat gain/loss and thereby temperature change in a PCP system is influenced by ambient conditions: air temperature, wind speed, relative humidity, precipitation, and solar radiation. According to a study by Flower et al. (2010), the temperature behavior of the PCP surface is also heavily influenced by the thermal properties of the material (e.g., thermal conductivity and heat capacity), whereas the surface temperature of traditional concrete and asphalt pavements are most heavily influenced by emissivity and solar radiation. It has been observed that PCP has a slower temperature response to daily meteorological indices (e.g., solar radiation, precipitation, and ambient temperature) compared with traditional concrete pavement (Flower et al. 2010). This behavior is attributed to the void structure of the material compared with traditional concrete pavement. The type of aggregate used in the PC mixture highly influences the thermal properties of PC and, therefore, influences the PCP nodal temperature. For example, during summer, the predicted daily peak temperature for limestone PCP was approximately 18°F higher than that of basalt PCP (Flower et al. 2010). The thermal properties of cement paste in PCP also influences the nodal temperature of PCP. Research by Fu and Chung (1997) showed that the specific heat of the cement paste is approximately 0.20 Btu/lb °F, which is the same specific heat as basalt, but is lower than that of limestone (Fu and Chung 1997, Goranson 1942). The air voids in PCP play a key role in the overall conductivity of PCP, because the *k* of air at 0.0024 Btu/ft^{2}hr ˚F is substantially lower than that of the paste and aggregate at room temperature (Çengel et al. 2008). Emissivity and solar radiation affect PCP temperatures. The maximum temperature fluctuations of PCP occur during the summer season,

when ambient temperature and solar radiation are the highest, while the magnitude of fluctuation drops drastically during overcast winter (Haselbach 2011, Boyer 2011, Kevern et al. 2009 b).

When PCP is evaluated in comparison with traditional PCC pavements, it stores less energy, even though the temperature of PCP is much higher than the temperature of traditional pavement during summer. This is due to the differences in physical properties (Kevern et al. 2012). Further, PCP cools more rapidly than traditional PCC pavement, suggesting that PCP has the potential to help dissipate the urban heat island effect (Haselbach 2011). However, Zhang et al. (2015) claim that the potential for PCP to mitigate the urban heat island effect is more dependent on the albedo of the pavement surface than on the evaporative cooling properties of the PCP. During early summer, the temperature of PCP is cooler than traditional concrete pavement, but the opposite effect occurs during late summer season. This behavior implies that a higher temperature in the base layer and in the soil affects the temperature of PCP by insulating it from cooling even though the ambient temperature has dropped (Boyer 2011). The temperature of soil gradually fluctuates on a seasonal cycle, but does not fluctuate daily, therefore providing a more stabilizing effect on PCP temperature (Kevern and Schaefer 2008, Kevern et al. 2009 b).

A study by Kevern et al. (2009 b) confirmed this behavior for the winter season. When ambient temperature is below freezing, the temperature of PCP remains higher than ambient temperature. The air in the base layer, acting as insulation and coupled with heat associated from the soil, helps to delay the formation of a frost layer under PCP (Kevern and Schaefer 2008, Kevern et al. 2009 b). The thawing behavior of PCP was also compared with traditional PCC pavement by Kevern et al. (2009 b), who found that thawing of PCP occurs approximately 1 month sooner than traditional concrete pavement. Therefore, winter maintenance operations of PCP may not be needed in the late winter season.

1.4.4. Thermal Properties and Heat Transfer of Pavement Systems

Three main types of heat transfer in pavement system can be described through radiation, convection, and conduction (Gui et al. 2007). With known thermal properties of pavement materials and heat transfer between layers, the temperature of pavement can be predicted with known heat sources applied at the pavement surface, which is primarily through net radiation from the sky (Gui et al. 2007). Heat transfer of the pavement system can be estimated using the heat transfer equation for a one-dimensional domain, where heat transfer is governed by the law of the conservation of energy, as presented in Equation 1-1 (Ye 2007).

$$\frac{d}{dx}\left(k \cdot \frac{dT}{dx}\right) + Q = \rho \cdot C_p \cdot \frac{dT}{dt} \qquad \text{Eq. 1.1}$$

where

k = Thermal conductivity, W/m/˚C or BTU/ft^{2}hr °F

T = Temperature, ˚C or ˚F

Q = Heat generated per unit time and volume, kW/m^3 or Btu/hr·ft^3

ρ = Density, kg/m^3 or lb/ft^3

C_p = Specific heat, J/kg/˚C or Btu/lb˚F

Temperature prediction for the pavement system at different depths throughout the pavement structure can be achieved by solving the heat transfer equation with respect to depth of the pavement, x and time, t (Nassiri 2011). The boundary conditions must be properly chosen to satisfy compatibility with the surrounding field conditions (Cook 2007). The heat exchanged between the pavement and the atmosphere is through conduction, convection, reflection, and absorption (Dempsey et al. 1985). Figure 1.1 presents heat transfer between the pavement surface and air on a sunny day.

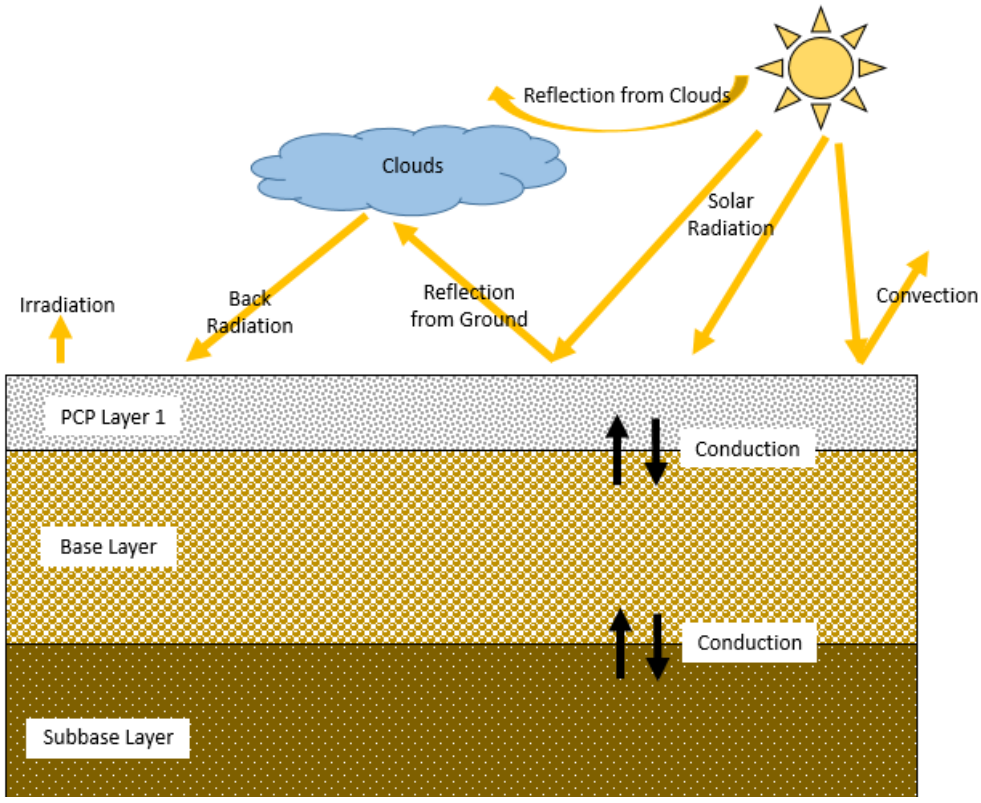

Figure 1.1 Heat transfer between the pavement surface and air on a sunny day (Dempsey et al. 1985)

Specific heat (Cp) and *k* are two key components for accurate predictions of heat transfer between the PCP and the atmosphere (Nassiri 2011). Specific heat is defined as the amount of heat required to raise the temperature of the unit mass of the material by one degree. Thermal conductivity is the heat that flows through the thickness of the material over a unit area (Harmathy 1970). In this study, the effective thermal properties of the PC was calculated by the parallel series method as a function of the thermal properties of each constituent and the volumetric fraction of each component, commonly used for rocks with various mineralogy (Equation 1.2.)

$$C_p = \sum(x_n C_n) = x_1 C_1 + x_2 C_2 + \cdots \qquad \text{Eq. 1.2}$$

where

x_n (n = 1, 2, …) = Percent volumetric of mineral content

C_n (n = 1, 2, …) = Specific heat corresponding to the constituent

Table 1.1 presents the Cp of different types of rock at cold and hot temperatures. The Cp in cold conditions would be relatively realistic for wintertime conditions. The hot conditions of Cp reported in Table 1.1 are unrealistically warm for temperate climates.

Table 1.1 Specific heat of common rocks at 32˚F and at 135˚F (Goranson 1943)

Type of Rocks	**Specific Heat, C_p (Btu/lb ˚F)**	
Temperature	**32˚F**	**135˚F**
Basalt	0.20	0.30
Diorite	0.20	0.29
Granite	0.19	0.27
Limestone	0.29	0.30
Marble	0.23	0.29
Quartzite	0.22	0.28
Sandstone	0.27	0.27

The rate of heat flow through concrete is dependent upon the thermal properties of the aggregate, the type of cement used in the mixture, the density, and the moisture level in the concrete (Harmathy 1970). The thermal conductivity of PCP can be calculated using the parallel composite model, similar to the calculation of *k*, as shown in Equation 1.3 (Robertson 1988).

$$k = \sum(x_n C_n) = x_1 k_1 + x_2 k_2 + \cdots \quad \text{Eq. 1.3}$$

where

x_n (n = 1, 2, …) = Percent volumetric of mineral content

k_n (n = 1, 2, …) = Thermal conductivity corresponding to the constituent

The thermal conductivity of different types of rocks varies based on mineral composition (Robertson 1988). **Error! Reference source not found.** presents the *k* of several common rocks.

Table 1.2 Thermal conductivity of common rocks

Type of Rocks	*k* (Btu/ft^2· hr· ˚F)
Basalt	0.85
Granite	0.98
Limestone	0.73
Marble	1.20
Sandstone	1.04

Because the estimates of the Cp and *k* of PCP are based on a simplified theoretical model, the thermal properties of traditional concrete were explored for baseline comparisons. The thermal conductivity of traditional PCC is sensitive to the mixture design because PCC is a composite material and the key components have different thermal properties. The conductivity of concrete can range from 0.87–2.1 Btu/hr·ft2·˚F, depending on aggregate type, w/cm, air content, and sometimes the admixtures (Hu et al. 2009). In addition, moisture conditions can influence the *k* of concrete. Table 1.3 provides a summary of the *k* of concrete at different moisture contents.

Table 1.3 Thermal conductivity of concrete in different moisture conditions (Lamond and Pielert 2006)

Type of Concrete	Moisture Content	Thermal Conductivities (Btu/hr·ft^2·°F)
Limestone Concrete	Moist	1.28
	50% RH	1.00
	Dry	0.81
Sandstone Concrete	Moist	1.68
	50% RH	1.28
	Dry	0.81
Quartz Gravel Concrete	Moist	1.91
	50% RH	1.57
	Dry	1.33
Expanded Shale Concrete	Moist	0.49
	50% RH	0.46
	Dry	0.36

Understanding the thermal properties of PCP and temperature trends of PCP during the winter season based on ambient indices can be used as groundwork for winter maintenance operations. The parallel series method of calculating thermal properties has been generalized to include aggregate, cementitious materials, and air. The actual thermal properties of PCP could include consideration of components such as fly ash, admixture, or other components included in the PC mixture, as well as moisture content. Calculated and measured values were compared, and measured values were used to model temperature trends in PCP. The information was used as input in the temperature prediction model to predict the temperature of PCP in laying the groundwork for future maintenance procedures.

CHAPTER 2. APPROACH

2.1 Laboratory Experiments

The objective of the laboratory experiments was to determine the thermal conductivity (*k*) of pervious concrete (PC) for different porosities. In doing so, *k* was determined using two different methodologies: heat flow analysis (FOX 304 heat flow meter) and heat impulse (RK-1 rock sensor kit). Tests on two different specimen types—slabs and cylinders—were conducted in both dry and wet conditions. The goals were to (1) develop a relationship between *k* and porosity; (2) evaluate the feasibility of using a portable device for thermal conductivity, which was developed for testing composite rocks; and (3) compare *k* in dry and wet conditions.

2.1.1 Mixing Pervious Concrete and Casting Slabs

Mixing Design

The PC mixture was designed to conform to the mixture design guidelines in ACI 522R-10 (ACI 2010). Several trial batches of PC were made, and the mixture design was modified to achieve the target porosity and strength. The final PC mixture design and proportions of the PC constituents are provided in **Table** 2.1.

Table 2.1 PC mixture proportions

Constituents	**Amount (lb/cu yd)**
Saturated Surface Dry Coarse Aggregate	2750
Fine Aggregate	0
Cement	570
Fly Ash	100
Water	160
Admixture (oz/cwt)	15

The PC was prepared with Type I/II ordinary portland cement and crushed basalt coarse aggregate. Coarse aggregate with a nominal maximum size of 3/8 inch, available at the local ready-mix supplier for pervious concrete, was used. The coarse aggregate had a specific gravity

of 3.102 and water absorption of 3.11%. No fine aggregate was included in the PC mixture. All coarse aggregate was first washed to clear it of debris and dust; it was then soaked for 24 hours and towel-dried to achieve saturated surface dry (SSD) conditions at the time of mixing. Fifteen percent of the portland cement by mass was replaced with Type F fly ash. A rheology-modifying chemical admixture, VMAR VSC500, provided by Grace & Co., was used in the mixture. This type of admixture is designed specifically for PC to enhance the rheology of the fresh mixture and to delay the time of set, providing a more workable time. Mixing and curing were followed by porosity, infiltration, and thermal conductivity testing.

Sample Preparation and Curing

The PC specimens were mixed in accordance with specifications found in the American Society for Testing and Materials (ASTM) C192-16a (ASTM International 2016). A rotary drum mixer was used to mix three PC batches of 0.78 cu ft. Mixing was preceded with "buttering" the mixer with 0.24 cu ft of an initial PC batch consisting of the same compounds as the test batches. Two types of specimens were cast: cylinders (4″ in diameter by 8″ in height) and slabs (11.25″ by 11.25″ by 3.25″).

The PC specimens were compacted to target a variety of porosity levels to determine the *k* of PC as a function of porosity. The compaction method for the cylinders was selected to result in uniformly compacted specimens through the cylinders' depth, ensuring the best possible uniform porosity throughout the specimen depth. The slabs were compacted to represent field placement and compaction procedure. Polyvinyl chloride (PVC) molds were used to cast the cylindrical specimens, and wooden molds were used to cast the slabs. The amount of fresh PC placed in each specimen mold was pre-determined using the designed porosity of the mixture and known volume of the mold. Cylindrical samples were filled with PC in two lifts. The bottom

lift was compacted with 15 blows of a 5.5-lb Proctor Hammer with a drop height of 12 inches. The mold was then filled to the top and compacted with the Procter hammer, using as many drops as was needed to fit the pre-determined weight of the mixture in the mold.

Slab molds were filled with fresh PC in one lift and initially compacted with about 33 blows of the same Proctor hammer to cover the entire surface area of the slab (Figure 2.1). To ensure consistent filling of the mold with fresh mix, the sides of the mold were hit with a plastic mallet all around the specimen. After the initial compaction, the slabs were statically compacted using a hydraulic compression testing machine, applying the load of about 700 lb (Figure 2.2). This method of compaction is different from the vibratory screed used in the field; however, it does recreate the top-down distribution of density. This load corresponds to Bunyan roller compaction of 49 lb over a 3-feet-wide roller compactor.

All specimens were cured in closed (capped) molds for 7 days in laboratory conditions, with ambient temperature of around 72˚F. After this period, all specimens were demolded and tested for porosity and infiltration, and then cured in air. The number of specimens cast from the PC mixture consisted of nine 4-inch cylinders and six slabs—fifteen specimens in total.

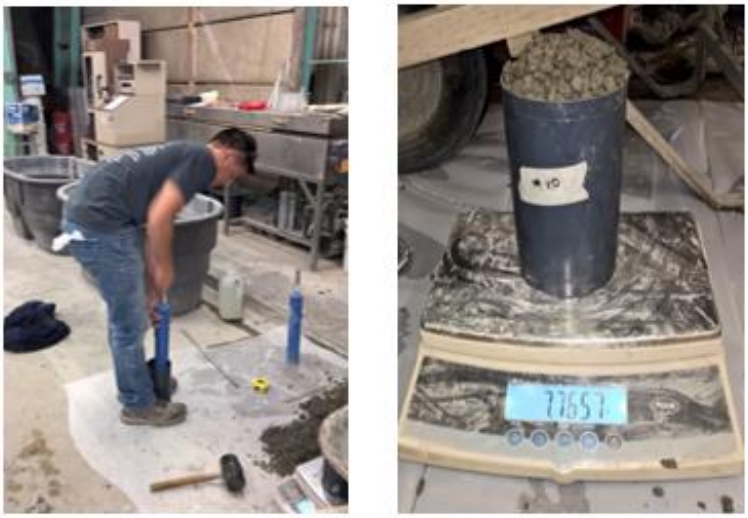

Figure 2.1 PC cylinder specimen compaction with Proctor hammer (left); the amount of fresh PC placed in each mold before compaction (right)

Figure 2.2 PC slab compaction in hydraulic compression testing machine (left); finished PC slab before curing (right)

2.1.2 Thermal Properties Characterization

The thermal conductivity of the specimens was determined by two methods: (1) heat flow meter and (2) sensor probe. The heat flow meter (model FOX 304 manufactured by LaserComp – TA Instruments, see Figure 2.3), which conforms to ASTM C518-15 (ASTM International 2015), was used to determine *k* in the first method. The heat flow meter measures the thickness of the specimen. A temperature gradient throughout the slab thickness is developed by setting different temperatures at the top and bottom plates of the heat flow meter container. Thermal

conductivity is determined based on the heat flow at known temperature gradients. Heat flow meter measurements of *k* were performed on slab specimens in dry conditions. The slabs were placed in the oven at 122°F for 12 hours before *k* testing to ensure fully dry conditions.

An RK-1 rock sensor probe along with the KD2 Pro thermal properties analyzer datalogger manufactured by Decagon Devices (Figure 2.3) was used to determine *k* in the second method. The 2-1/3-inch-long and 1/6-inch in diameter RK-1 sensor probe is designed to measure the *k* and thermal resistivity of rock, concrete, and other solid and composite materials. The sensor is connected to the KD2 Pro thermal properties analyzer datalogger to establish the sensor settings and collect the data. The sensor applies a heat impulse to the specimen during a 15-minute period, as recommended by the manufacturer. After the 15-minute period, the result of the *k* test is automatically saved in the KD2 Pro. Sensor probe *k* measurements were performed on cylindrical specimens only in dry conditions, and on slabs in both dry and wet conditions.

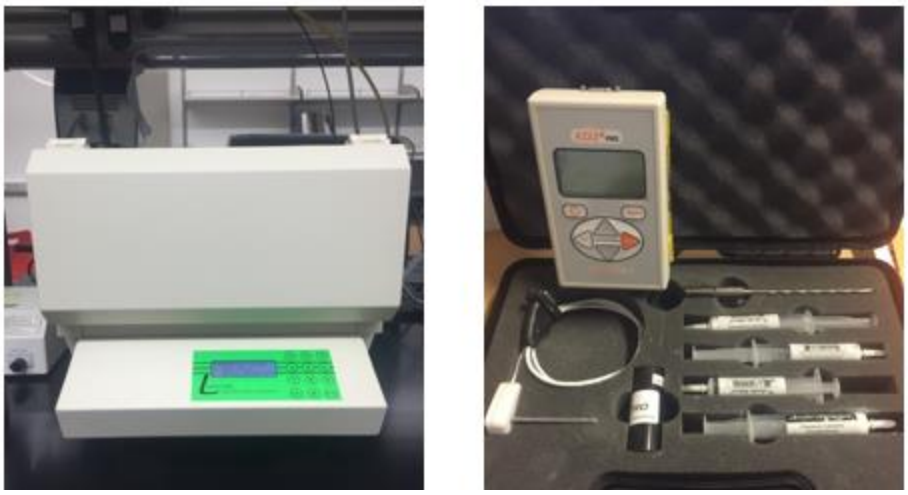

Figure 2.3 FOX 304 heat flow meter (left); RK-1 rock sensor kit and KD2 Pro analyzer (right)

2.1.3 Porosity and Infiltration Testing

Upon demolding the specimens at 7 days of age, porosity and dry density were determined in accordance with ASTM C1754-12 (ASTM International 2012). Total void content

was estimated as the difference between the total volume of the sample and the volume of the displaced water when the sample was submerged, using Equation 2.1. The volume of the specimens was estimated based on the average dimensions (height and diameter of the cylinders; width and height of the slabs) obtained from three measurements using a caliper.

$$Total\ Void\ Content = (1 - \frac{M_w - M_d}{\rho_w \cdot V}) \quad \text{Eq. 2.1}$$

where

M_w = Mass of submerged specimen, g

M_d = Mass of a dry specimen, g

ρ_w = Density of water, g/cm^3

V = Volume of the specimen, cm^3.

Infiltration is a critical property of PCP for stormwater applications. Therefore, infiltration rates of the PC specimens were determined following ASTM C1701-09 (ASTM International 2009). Modification was made to the ASTM procedure by using a smaller ring instead of the 12-inch ring used for field testing. Cylindrical specimens were wrapped on the sides with shrink-wrap, which simulated a columnar test setup. Shrink-wrap enabled the water to be poured from the top and exfiltrated at the bottom without loss at the sides (Figure 2.4). Infiltration rate tests were conducted with 1 liter of water for the 4-inch cylinders. The infiltration rate of cylindrical specimens was determined based on two subsequent measurements that followed pre-wetting. The infiltration rate of slab specimens was determined using the 4-inch infiltration ring, fastened to the slab by plumber's putty (Figure 2.4). The infiltration test was performed with 1 liter of water, at 4 different locations on each slab. Every infiltration test on the slab was preceded with pre-wetting. The infiltration rate of slabs was reported as the

average of measurements from four different locations on each slab. Calculation of infiltration is represented in Equation 2.2.

$$I = \frac{V}{t \cdot A} \qquad \text{Eq. 2.2}$$

where

I = Infiltration, inch/hr

t = Time, sec

A = Surface area, in^2.

Figure 2.4 Infiltration test performed on 4-inch PC cylinder (left) and on PC slab (right)

2.2 Field Data Collection

The objective of the field experiment was to observe the temperature of a PCP installation exposed to ambient conditions in Pullman, Washington. Temperature sensors were embedded in the PCP at different depths to collect temperature data over time. The temperature of the PCP was compared side-by-side with the ambient temperature to identify the freezing periods of PCP with respect to ambient temperature. The temperature data were also used as baseline measured temperatures to evaluate the accuracy of the predictions for PCP temperature.

2.2.1 Project Location

A 26-foot-long PCP sidewalk was placed in front of the Duncan Dunn/Community Residence Hall on Washington State University (WSU) – Pullman campus in May 2015. The project, a sidewalk reconstruction conducted by WSU's Facility Services, is located at 720 NE B St. in Pullman. Figure 2.5 shows the project section with a red strip, indicating the location of the PCP sidewalk.

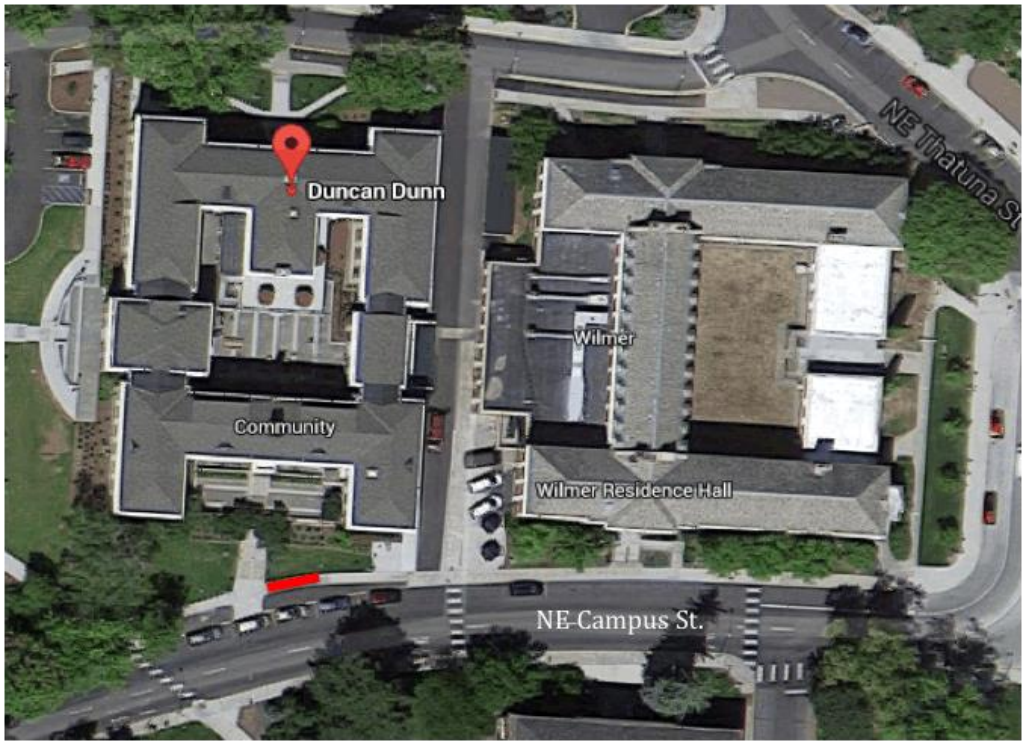

Figure 2.5 Map image of the project location (Google Map. Retrieved in 2015)

2.2.2 Installation of PCP Sidewalk and Instrumentation

The existing asphalt sidewalk was replaced with PCP produced and delivered by Atlas – Sand, Rock, and Concrete from Pullman, Washington. The contractor responsible for this construction project was William Winkler Construction Company. The mixture design proportions of the PCP provided by Atlas are presented in Table 2.2. The design w/cm and the void content were 0.32% and 20%, respectively.

Table 2.2 Mixture design of PC used to pave the sidewalk

PCP Constituent	Amount (lb/yd^3)
Coarse Aggregate – Limestone	2,798
Fine Aggregate	None
Cement	500
Water	110
Admixture (oz/ctw)	15

PCP Construction

The PC sidewalk construction started at around 12:30 PM on May 20, 2015. The conditions were sunny with ambient temperature of 68˚F and humidity of 19%. The pouring and placing of the PCP took 3 hours from start to finish; compaction of the PCP sidewalk began as soon as the pouring started. Presented in Figure 2.6 are the steps taken during construction. A 3-foot-long Striker roller screed weighing 49 lb (manufactured by Banyun Industries) was rolled three times over the pavement surface for compaction (Figure 2.6a). The edges of the PCP sidewalk were smoothed by hand finishing (Figure 2.6b). Once compaction was completed, 4-foot contraction joints were cut in the pavement using a roller joint cutter, also manufactured by Banyun Industries (Figure 2.6c). Finally, the PCP sidewalk was covered with a polypropylene sheet, secured with 2- by 4-inch lumber, for curing. The polypropylene sheet was left on the sidewalk for 7 days before the sidewalk was opened to public use (Figure 2.6d).

Figure 2.6 (a) Compacting PC pavement surface using a roller screed, (b) hand finishing the pavement edge, (c) cutting pavement joints with a roller joint cutter, (d) polypropylene sheet covering the PC sidewalk for curing

Instrumentation and Data Collection

Nine sensors were installed throughout the depth of the PCP slab. Two of the nine sensors—Time Domain Reflectometer (TDR) sensors manufactured by Decagon Devices, Inc.—measured moisture and temperature. The other seven sensors were thermocouple wires (manufactured by Omega Company), which measured the temperature within the PCP.

Two series of thermocouple and TDR sensors were securely tied along the 6-inch length of a wooden dowel, referred to as the "sensor tree," to measure the temperature of the PCP at

various depths. Two sensor trees were made: one consisting of four sensors and one consisting of five sensors. The sensor trees were planted in two locations along the 26-foot PCP sidewalk. Both sensor trees were installed on the centerline of the sidewalk, one at 2 feet and the other at 10 feet from the west edge of the sidewalk, labeled Sensor Tree A and Sensor Tree B, respectively, in Figure 2.7.

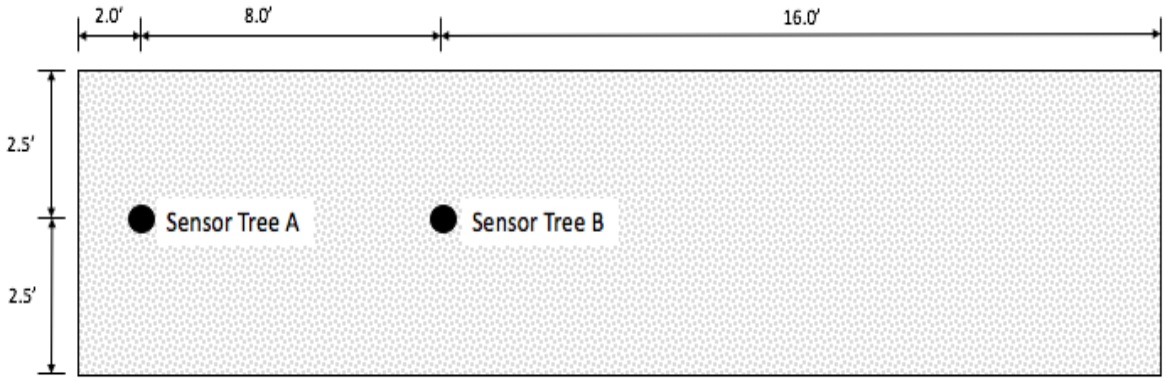

Figure 2.7 Location of sensor trees with respect to the PCP sidewalk boundaries – plan view

The sensor series on Sensor Tree A were located at 0.5-, 1.5-, 2-, and 3-inch depths from the surface of the PCP sidewalk. The sensor series on Sensor Tree B were located at 0.5-, 1.5-, 2-, 3-, and 5.5-inch depths from the surface of the PCP sidewalk. The TDR sensors were installed at 3-inch depth on each of the sensor trees, and thermocouple sensors were installed at all other depths. Figure 2.8 illustrates the location of the sensor trees and the sensors in a cross-sectional view of the 6-inch-thick PCP sidewalk. Figure 2.9 shows the setup of a sensor tree in the river rock base course just before the placement of the PCP sidewalk.

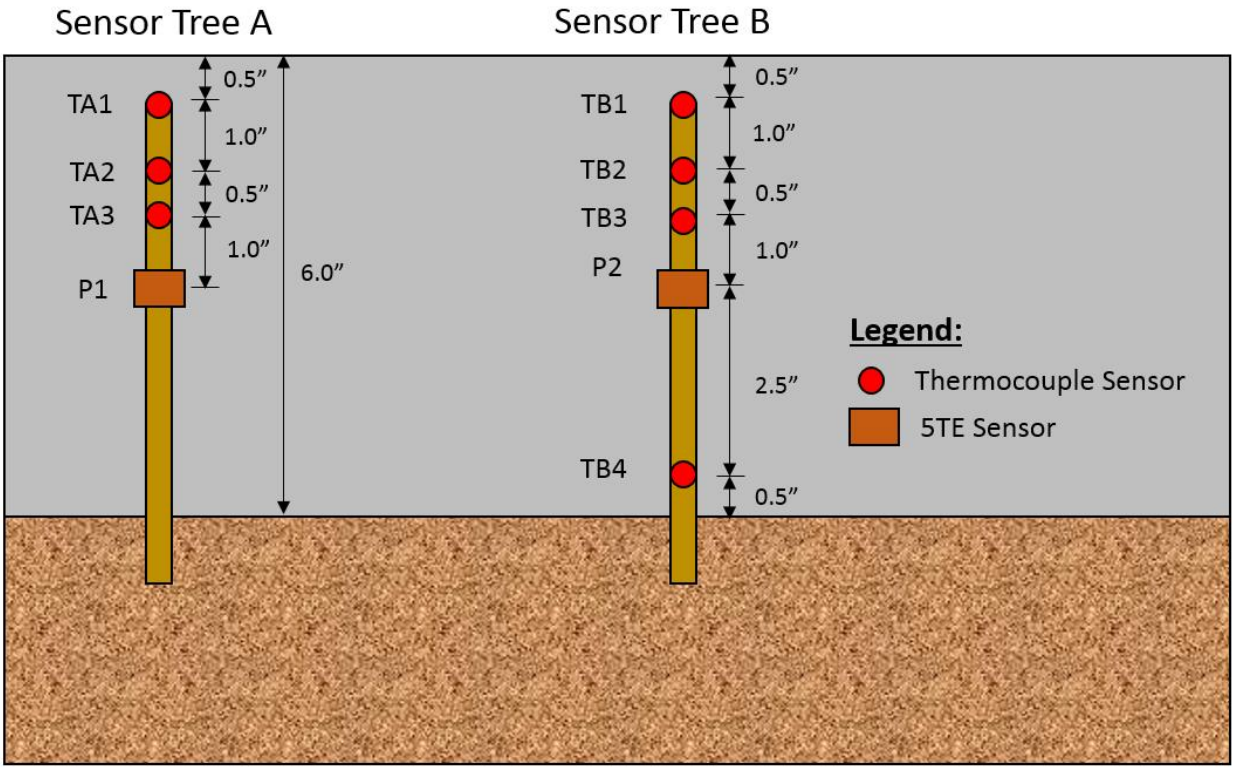

Figure 2.8 Layout plan of sensor trees and sensor locations with respect to PCP

Figure 2.9 Sensor tree before the placement of the PC sidewalk

To ensure that each sensor tree stayed in its intended position, small portions of PC were hand-placed and lightly compacted around the sensor trees and their wires before the rest of the sidewalk was poured. Sensor wires outside the PC sidewalk boundary were buried 1 foot underground inside a 2-inch-diameter PVC pipe, which crossed a grass lawn to the datalogger.

Ambient data including temperature, relative humidity, and wind speed were collected by a local weather station about 0.5 mile from the project site. Ambient data were collected through AgWeatherNet, an automated weather station overseen by the College of Agriculture, Human, and Natural Resource Sciences at WSU. Additionally, a pyranometer (solar) sensor manufactured by Campbell Scientific (model CS 300-L) was installed at the project site 47 days after the construction of the PCP on July 7, 2015. The pyranometer was fixed on a 3-foot extended arm attached to a streetlight post 10 feet off the northwest corner of the sidewalk. The pyranometer was located 7 feet from the ground on the light post, facing south toward the sidewalk. The radiation captured at the project site accounts for the absorptivity of the atmosphere and reflective radiation under cloud-cover conditions.

All nine sensors on the sensor trees plus the pyranometer were connected to a CR1000 Measurement and Control Datalogger system by Campbell Scientific, Inc. for data storage and collection. The datalogger operates on WSU's intermittent power supply for the light post, which is lit during the night. The datalogger's 12-volt PS 200 battery by Campbell Scientific Inc. was charged during the night and used as a steady-state power source for the system. The pavement and solar radiation data were recorded and stored in the datalogger in 15-minute intervals for 24 hours per day. Field data were gathered manually every 2 weeks. Figure 2.10 shows the location of the sensor instrumentation with respect to the PCP sidewalk boundary and the datalogger box.

Figure 2.10 Project boundary showing location of sensor trees (green dots on the sidewalk), solar sensor (red circle) and datalogger (red box) with respect to the PC sidewalk (red dashed line).

CHAPTER 3. DATA ANALYSIS

3.1 Porosity and Infiltration Results and Analysis

Porosity was determined in the laboratory for all specimens at 7 days of age, immediately after demolding. Figure 3.1 shows the range of porosity of the six slabs. The porosity of the six slab specimens ranged from 18% to 36%.

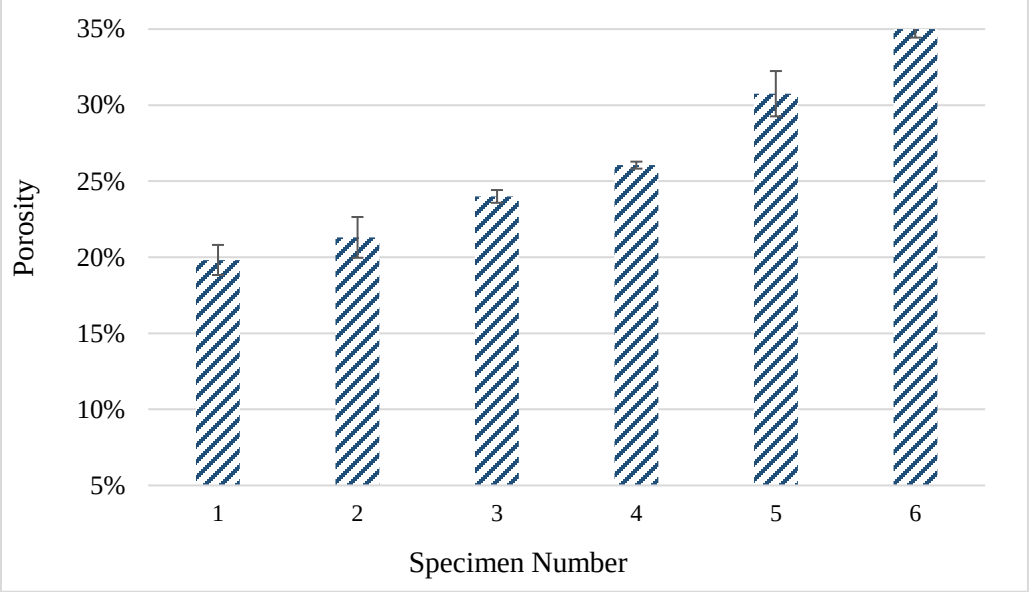

Figure 3.1 Hardened porosity of slab and cylindrical specimens

Note that the porosity of PC specimens varies with depth due to the current compaction practice (roller compaction from top-down) for PCP casting and placement. Low porosity (higher density) is typically found a few inches at the top from the PC surface, while porosity increases as depth increases for PC that is compacted only from the surface (Haselbach and Freeman 2006). Therefore, after initial porosity characterization for the cylinders, these specimens were saw cut at mid-depth. The porosity values of the top and bottom halves versus the porosity of whole specimens are presented in Figure 3.2.

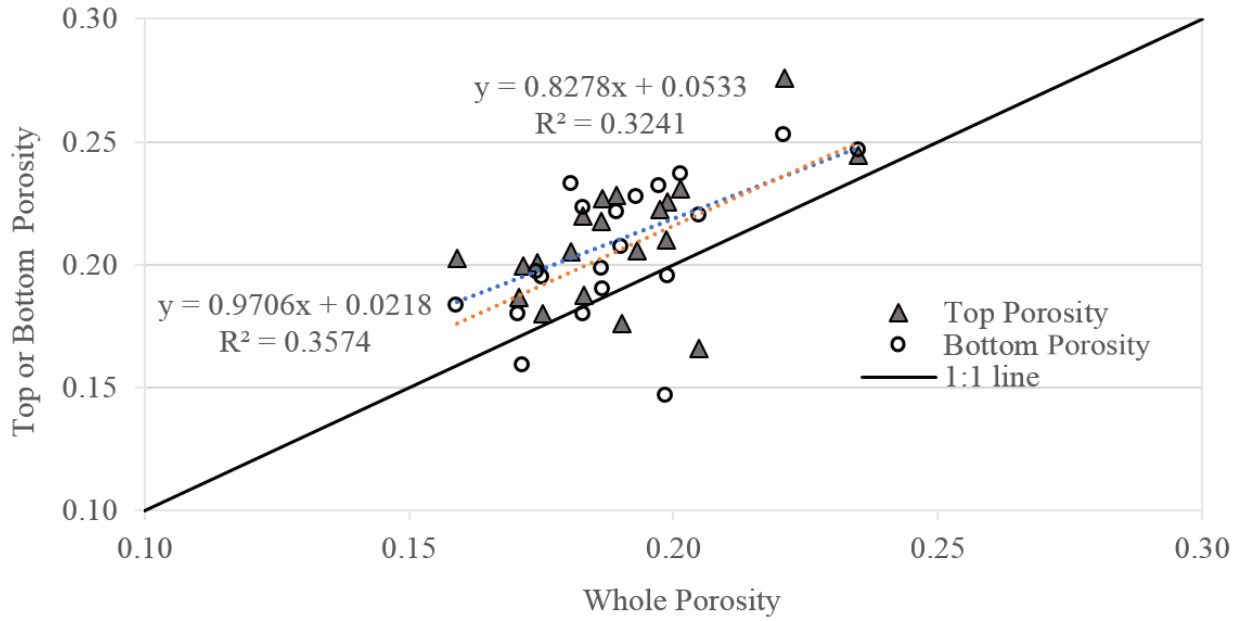

Figure 3.2 Porosity of top and bottom cylinders versus porosity of whole specimens

According to Figure 3.2, the porosity of the whole cylinders ranged from 16% to 23%. The linear regression fit to the data shows that the top halves compacted to 83% of the whole porosity plus 5%, and the bottom halves yielded 97% of the whole porosity plus 2%. These results show that the cylinders were reasonably uniformly compacted throughout depth; however, the bottom cylinders were more closely compacted to the whole porosity. This behavior is expected, since some of the compaction energy is transferred to the bottom halves when the cylinder is being compacted at the top, resulting in more compaction of the bottom half. Furthermore, the bottom halves show slightly higher variation in compaction, with a coefficient of variation of 0.137 versus 0.121 for the top halves.

Infiltration tests were conducted on all slabs at 7 days of age after porosity testing. Figure 3.3 shows that a strong linear correlation ($R^2 \geq 0.92$) between porosity and infiltration can be established. The average infiltration values for all specimens are 1,000 to 4,250 inches-per-hour and are within the typical range for PC (300~2,000 in/h) (ACI 522R-10 [ACI 2010]).

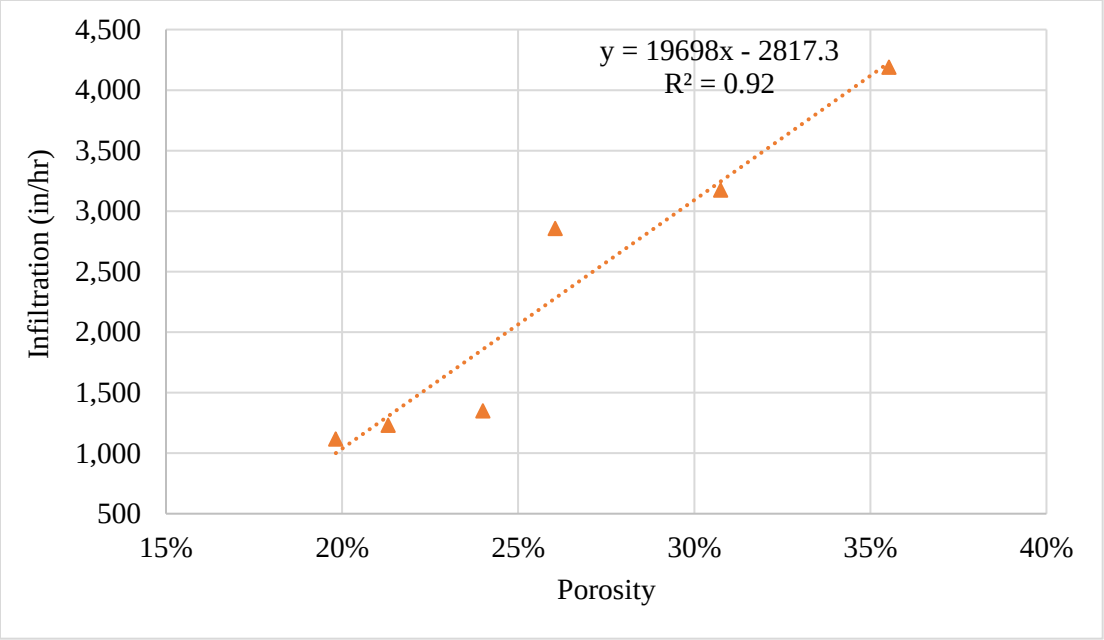

Figure 3.3 Correlation between porosity and infiltration of PC slabs

3.2 Thermal Properties Results and Analysis

3.2.1 Thermal Conductivity Test Results – Dry PC Cylindrical Specimens

As mentioned before, due to the shape and size restrictions of the heat flow machine, the *k* of the cylindrical specimens was only determined using the RK-1 sensor probe. Figure 3.4 presents the average *k* (from four test repetitions) for the dry cylindrical specimens with their corresponding porosity. Results in Figure 3.4 show a declining trend in *k*-porosity for cylinders. The line fitted to the top halves has a less steep slope than the line fitted to the bottom halves, possibly due to the wider range in φ for the bottom halves, as discussed previously. The bottom halves show a wider range in *k*, 0.37–0.58 W/(mK); this range for top halves is 0.46–0.62 W/(mK). This behavior could be due to a higher number of bottom halves with porosity greater than 22% compared with the top halves, given that the disparity between the top and bottom values increases at higher porosity levels. On average, the *k* of the bottom halves is 0.49, and the *k* of the top halves is 0.56 W/(mK). More discussion is available in (Nassiri and Nantasai 2017).

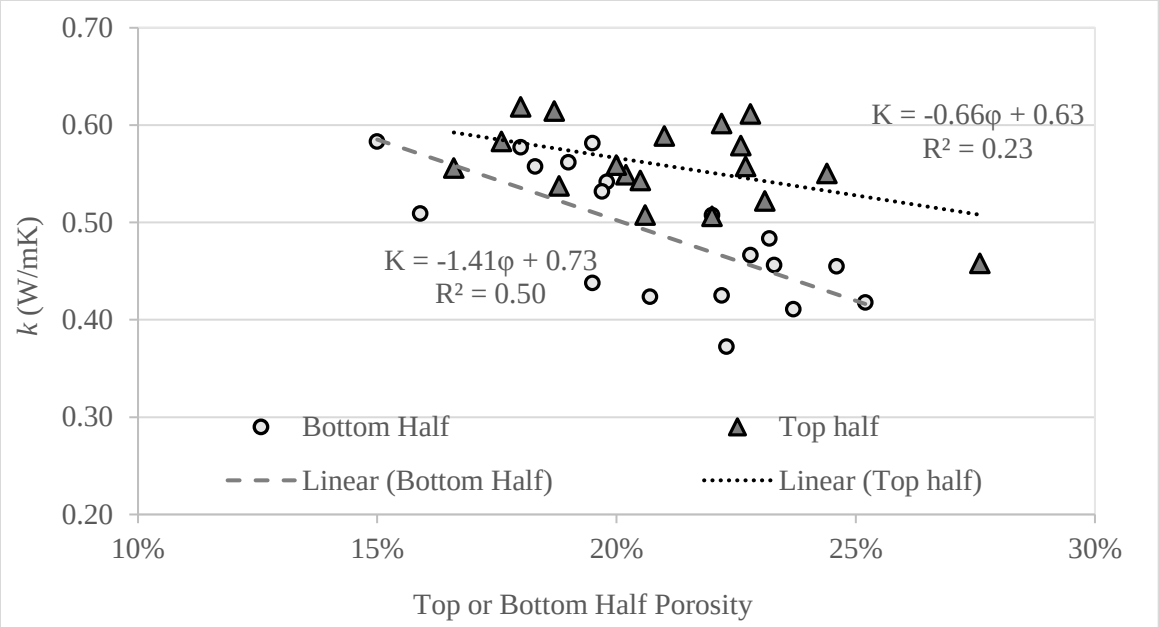

Figure 3.4 Average *k* of dry cylindrical specimens determined by the RK-1 sensor probe, W/(mK) = 1.7307 × Btu/(hr ft ˚F).

3.2.2 Thermal Conductivity of PC Slabs in Dry Condition

The thermal conductivity of slabs in dry condition was tested with both the FOX 304 heat flow meter and the RK-1 sensor probe. The results of *k* are consistent among different test temperatures for both methods, as indicated in Table 3.1. The values of *k* captured by the FOX 304 heat flow meter are approximately 10% lower than those obtained from the RK-1 sensor probe. The average values of *k* from the two methods are shown in Figure 3.5 in comparison with the line of equality. Again, it is evident that the data using both devices are compatible.

Table 3.1 Thermal conductivity results obtained from the FOX 304 heat flow meter and the RK-1 sensor probe

		FOX 304 Heat Flow Meter			RK-1 Sensor Probe		
Porosity	Test Trial	Average Test Temperature (°F)	Measured *k* (Btu/hr·ft·°F)	Average *k* (Btu/hr·ft·°F)	Average Test Temperature (°F)	Measured *k* (Btu/hr·ft·°F)	Average *k* (Btu/hr·ft·°F)
20%	1	144.5	0.37	0.37	67.05	0.41	0.44
	2	126.5	0.37		66.97	0.47	
	3	108.5	0.37		67.06	0.50	
	4	90.5	0.36		67.39	0.41	
	5	Not Tested	Not Tested		67.39	0.43	
22%	1	144.5	0.33	0.32	67.15	0.37	0.42
	2	126.5	0.32		66.85	0.47	
	3	108.5	0.32		67.10	0.36	
	4	90.5	0.31		66.79	0.47	
	5	Not Tested	Not Tested		67.15	0.43	
24%	1	144.5	0.33	0.33	Not Tested	Not Tested	Not Tested
	2	126.5	0.33		Not Tested	Not Tested	
	3	108.5	0.33		Not Tested	Not Tested	
	4	90.5	0.32		Not Tested	Not Tested	
	5	Not Tested	Not Tested		Not Tested	Not Tested	
26%	1	144.5	0.25	0.24	66.38	0.34	0.33
	2	126.5	0.24		66.06	0.34	
	3	108.5	0.23		66.22	0.38	
	4	90.5	0.23		66.52	0.31	
	5	Not Tested	Not Tested		66.47	0.27	
30%	1	144.5	0.28	0.27	65.80	0.27	0.31
	2	126.5	0.28		65.93	0.37	
	3	108.5	0.27		66.13	0.23	
	4	90.5	0.27		68.58	0.34	
	5	Not Tested	Not Tested		65.55	0.34	
35%	1	144.5	0.22	0.21	65.77	0.28	0.28
	2	126.5	0.21		65.55	0.29	
	3	108.5	0.21		65.55	0.26	
	4	90.5	0.20		65.61	0.24	
	5	Not Tested	Not Tested		65.43	0.31	

Note that the thermal conductivity of the slab with 24% porosity was not established because this slab was prepared as part of another project and could not be damaged by drilling for RK-1 sensor probe testing.

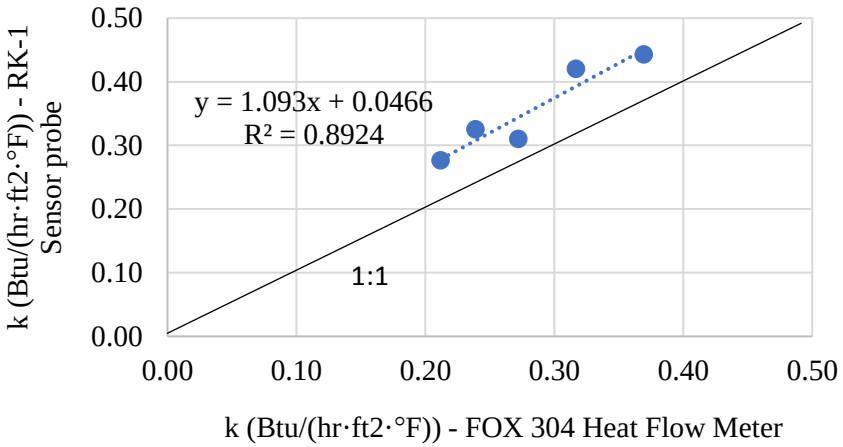

Figure 3.5 Comparison of average *k* of dry PC slabs obtained from the RK-1 sensor probe and the FOX 304 heat flow meter

From Figure 3.6, the results of *k* obtained by both methodologies present strong linear relationships with porosity, represented with similar trend-line slopes. For the PC slabs with porosity ranging from 20% to 35%, the RK-1 sensor probe measurements show that *k* ranges from 0.29 to 0.43$\frac{Btu}{hr \cdot ft^2 \cdot °F}$, while the FOX 304 heat flow meter measurements show that *k* ranges from 0.21 to 0.37$\frac{Btu}{hr \cdot ft^2 \cdot °F}$. This difference is due to the difference between the two methodologies. The FOX 304 heat flow meter captures the thermal properties of the slabs by analyzing the entire depth from the slab top to bottom with the various heat steps. The *k* obtained by the RK-1 sensor probe is based on the contact area that the probe made with the specimen. Since the length of the probe is 2.33 inches, the bottom 1.67 inches of the slab were neglected. Therefore, the data captured by the two methods are not exactly comparable.

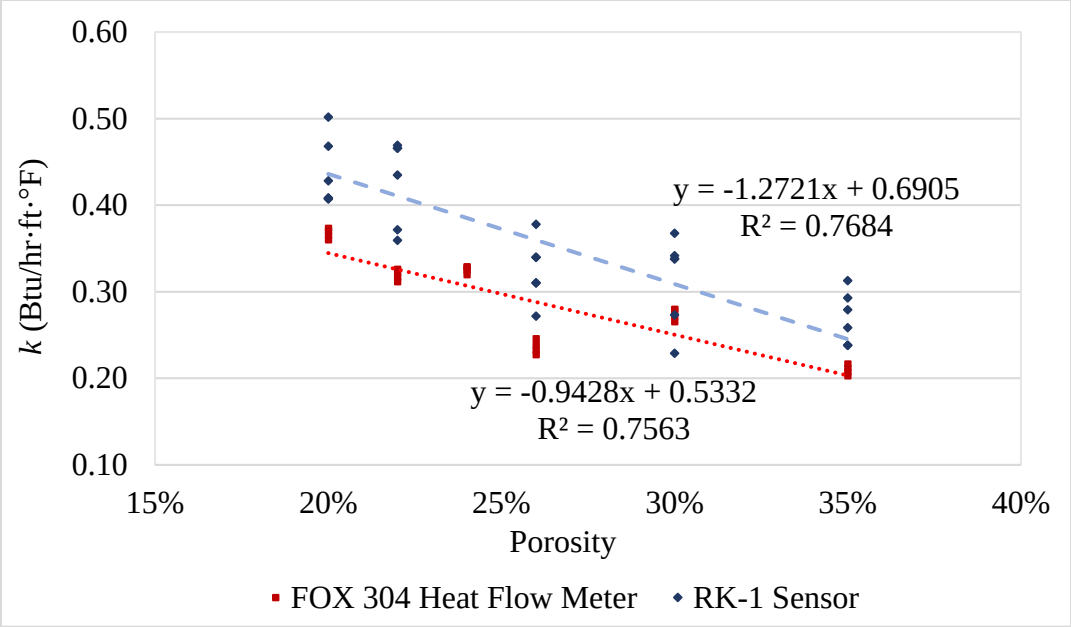

Figure 3.6 The relationship between average *k* and the porosity of dry PC slabs determined by the RK-1 sensor probe and the FOX 304 heat flow meter

3.2.3 Thermal Conductivity of PC Slabs in Wet Condition

The thermal conductivity of slabs in wet condition was tested with the RK-1 sensor probe in the curing room. Figure 3.7 presents the average values of *k* for PC slabs in dry and wet conditions, with corresponding standard deviations. As expected, values of *k* for the PC slabs in wet condition were higher than the values in dry condition. This is due to the conductivity of the water (Fricke 1992) and the fact that water trapped in the voids increases the contact area between the probe and the PC slab (Kim et al. 2003). The measured *k* of wet slabs ranges from 0.33 to 0.49$\frac{Btu}{hr \cdot ft^2 \cdot °F}$. A strong *k*-porosity correlation can be established for both dry and wet PC slabs (Figure 3.8).

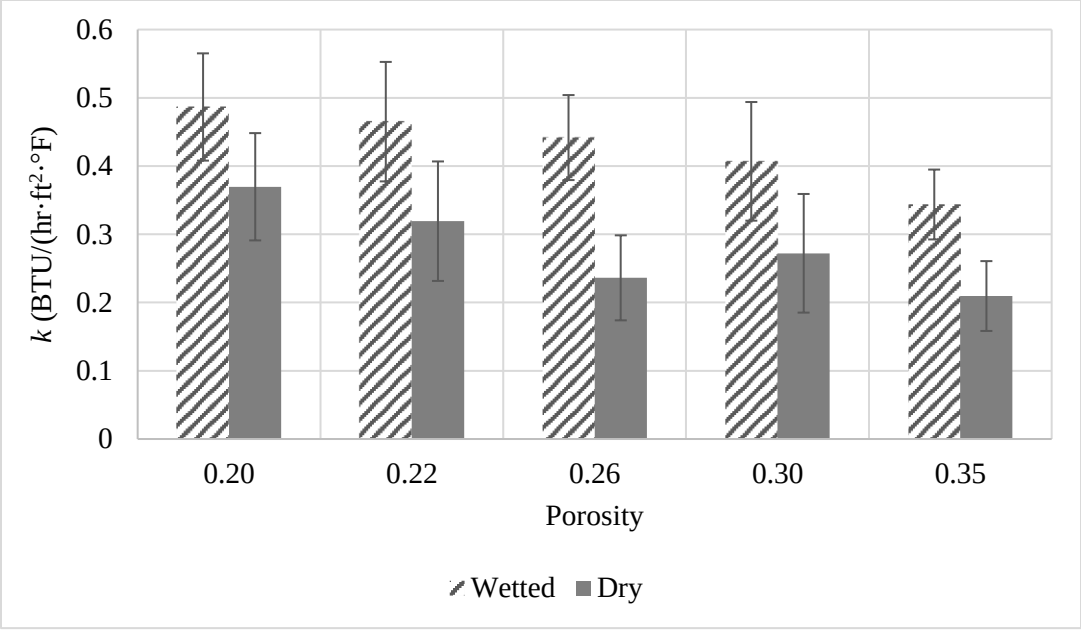

Figure 3.7 Thermal conductivity of PC slab specimens in dry and wet condition determined by the RK-1 sensor probe

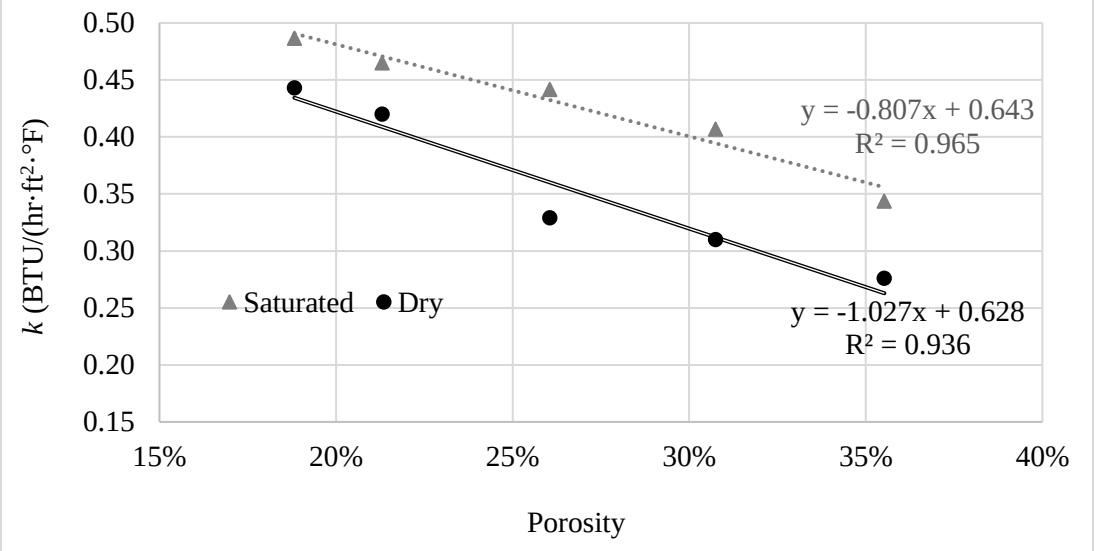

Figure 3.8 Relationship between the porosity and the average *k* of PC slab specimens in dry and wet condition determined by the RK-1 sensor probe

3.2.4 Prediction of Thermal Conductivity

Since laboratory characterization of *k* for different PCP mixtures is not always feasible, theoretical models for predicting *k* were explored. The thermal conductivity of PCP was calculated using the geometric parallel model (Equation 3.1). The thermal conductivity equation

has been generalized for PCP to account for the percent volumetric fraction and the *k* of three main components: aggregate, concrete paste, and air void. The percent volumetric fraction was obtained from the PCP mixture design.

$$logk_p = X_{agg} logk_{agg} + X_{paste} logk_{paste} + X_{air} logk_{air} + \cdots \quad \text{Eq. 3.1}$$

where X_{agg}, X_{paste}, and X_{air} are the volumetric fraction of aggregate, cement paste, and air, respectively, and k_{agg}, k_{paste}, and k_{air} are thermal conductivity of aggregate, paste, and air.

Table 3.2 shows the *k* of each constituent of PCP used for the calculation. Figure 3.9 presents the predicted and measured *k* of both dry and wet slabs.

Table 3.2 Thermal conductivity of constituents of PCP based on the literature
W/(mK) = 1.7307 × Btu/(hr ft ˚F)

Constituent	Thermal Conductivity (W/ mK)	Reference
Basalt Aggregate	1.69	Eppelbaum et al. (2014)
Cement Paste	0.98	Kim et al. (2003)
Air Void	0.026	Cengel et al. (2008)
Water	0.63	

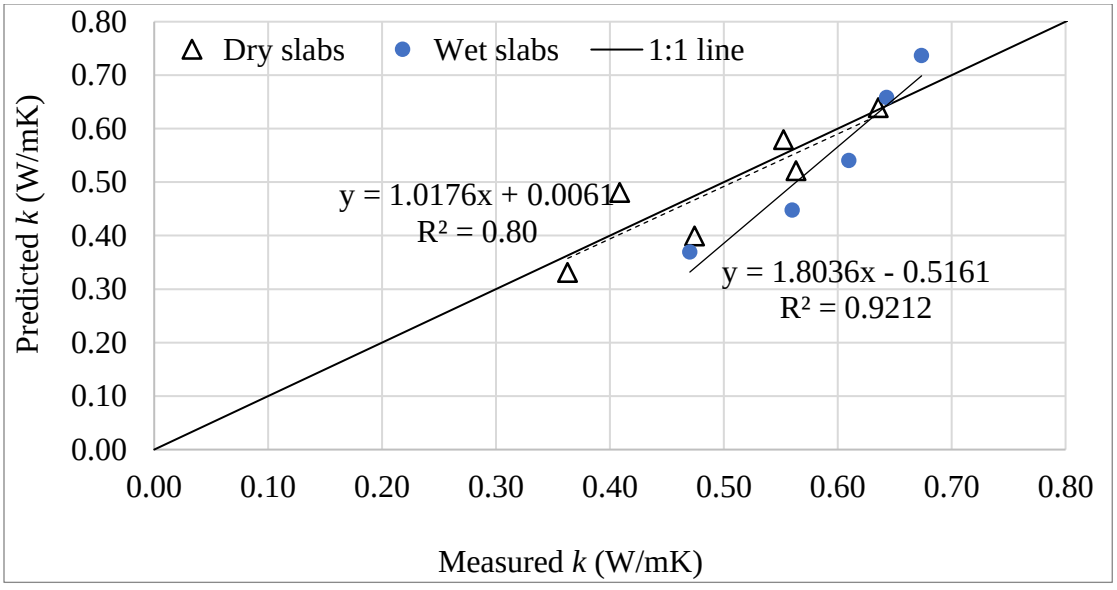

Figure 3.9 Comparison of *k* obtained by calculation and the FOX 304 heat flow meter

The predictions were close to the experimental data for two slabs and under-predicted by a maximum of 0.1 W/(mK) for the three slabs with higher porosity. The MSE of the model is 0.005 W/(mK). Overall, it is expected that the model's prediction for wet condition is not as good as its prediction for dry condition. The addition of water as one of the variables in the model is a simplistic approach. In reality, the water not only wets and partially fills the large air pockets in the PC, but also fills the various pores of the aggregate and paste, depending on the exposure duration, which alters each constituents' conductivity.

Using the same conductivity for the constituents in the mixture, the effective *k* was predicted for the top and bottom halves of the cylindrical specimens. The goodness of fit of the model to the experimental data can be seen in Figure 3.10. The predicted *k* of the top halves follows the line of equality closer than the predicted *k* of the bottom halves. The MSE for the top halves is only 0.003 m/Wk. however, *k* is over-estimated for all bottom halves; the average predicted *k* for the bottom halves is 0.60 W/(mK), while the measured value is 0.49 W/(mK), with MSE 0.012 W/(mK).

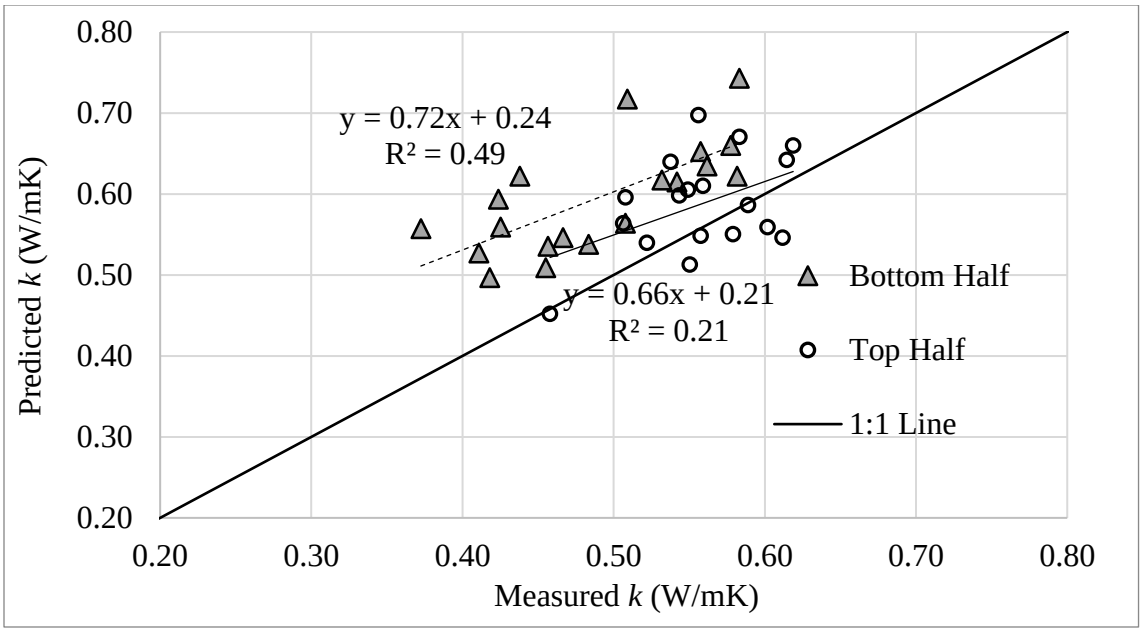

Figure 3.10 Fit of geometric mean parallel model of experimental *k* data for top and bottom halves of cylinders by needle probe method- W/(mK) = 1.7307 × Btu/(hr ft ˚F)

3.3 Field Data Analysis

3.3.1 Ambient Temperature and Solar Radiation Data Analysis

This section contains a discussion of the data collected for ambient temperature, solar radiation, and the temperature of PCP at 0.5-, 1.5-, 2-, and 3-inch depths from May 21, 2015, to April 4, 2017. The data are categorized by season: data from March through May are considered "spring"; from June through August, "summer"; from September through October, "fall"; and from November through February, "winter." Ambient temperatures were recorded for the same period as the temperature of the PCP, and solar radiation was recorded upon installation. Figure 3.11 shows the ambient temperature retrieved from the AgWeatherNet weather station and the solar radiation data captured at the project site. A solar radiation sensor was installed at the project site. The solar radiation followed a daily cycle, increasing during the day and decreasing to zero at night. Moreover, high ambient temperature and high solar radiation were observed

during the summer and fall seasons. The ambient temperature and solar radiation dropped significantly during the winter season.

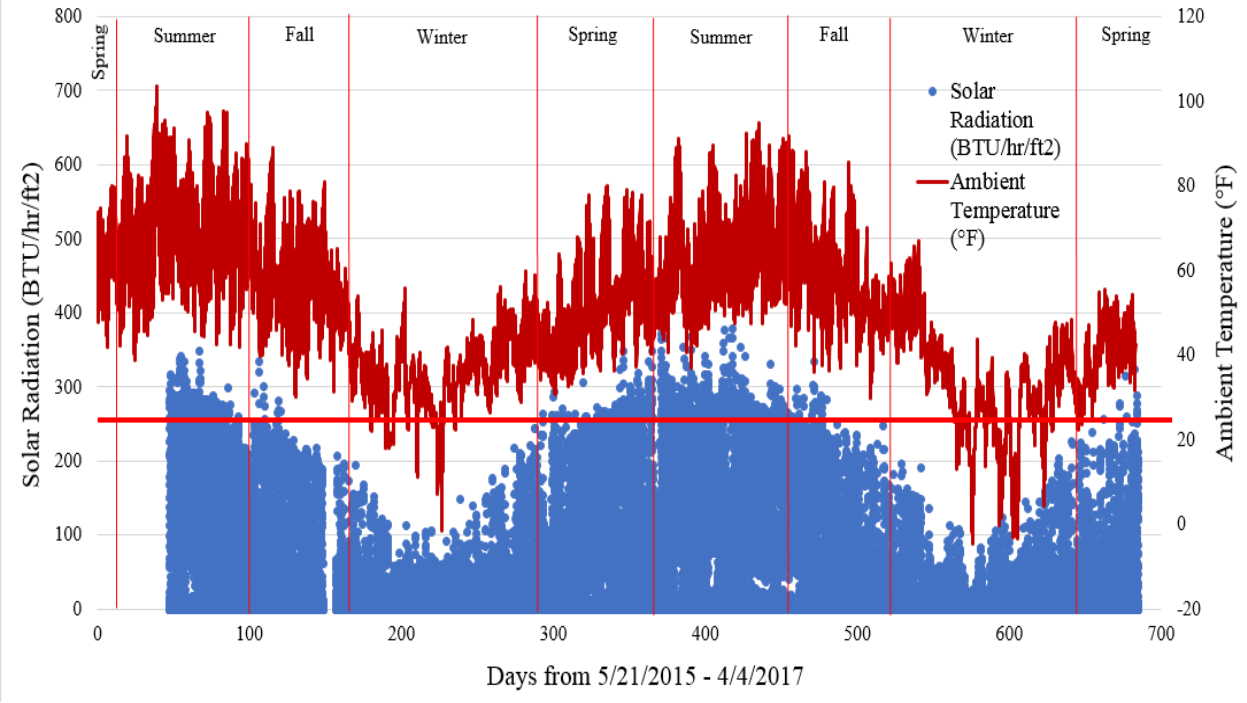

Figure 3.11 Ambient temperature and solar radiation data for the project site

3.3.2. Pavement Temperature Data

Figure 3.12 through Figure 3.15 show temperature comparisons of PCP from Sensor Tree A and B at 0.5, 1.5, 2, and 3 inches, respectively. The red horizontal line in each of these figures indicates temperature at 32°F. As seen in Figure 3.12, the PCP temperature at 0.5-inch depth captured from Sensor Tree A and B shows small variations. The maximum temperature difference between Sensor Tree A and B is less than 5°F. Similar conclusions can be drawn for the PCP temperature profiles at 1.5-, 2-, and 3-inch depth as indicated in Figure 3.13, Figure 3.14, and Figure 3.15, respectively.

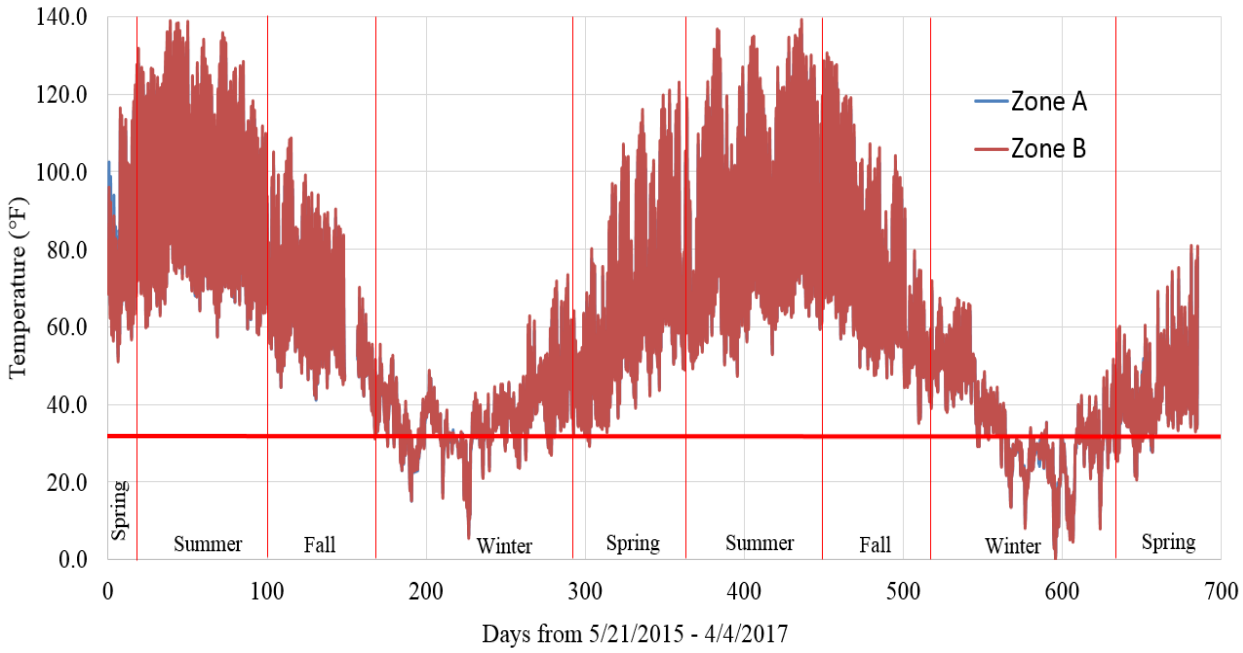

Figure 3.12 PCP temperature from Sensor Tree A and B at 0.5-inch depth

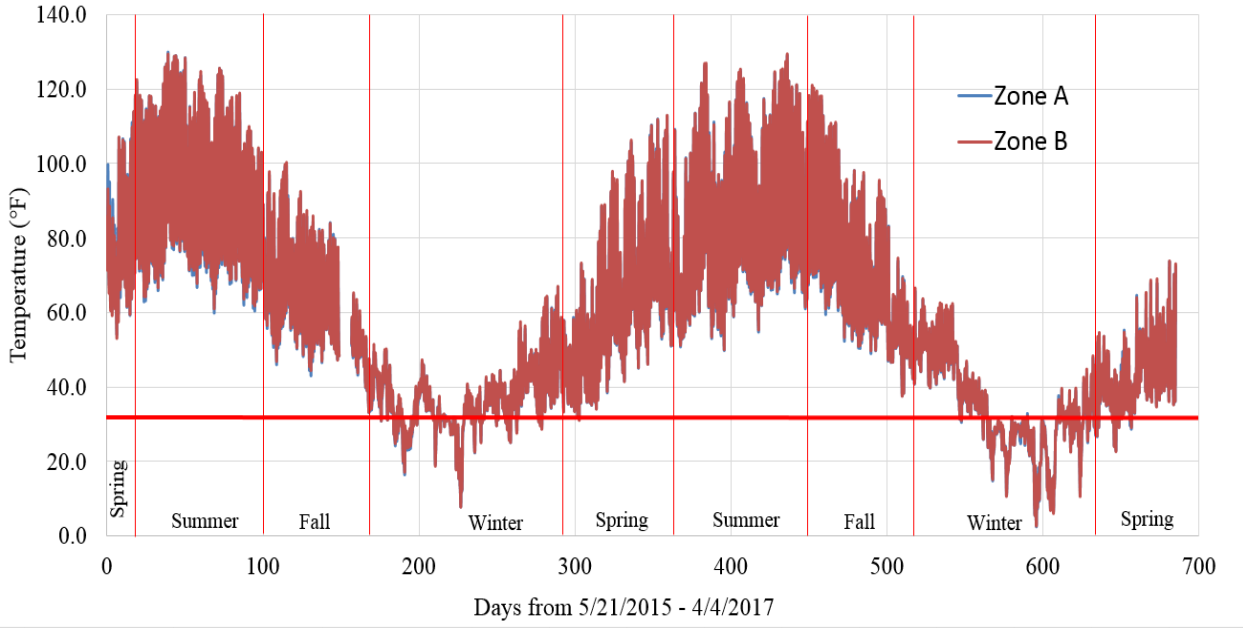

Figure 3.13 PCP temperature from Sensor Tree A and B at 1.5-inch depth

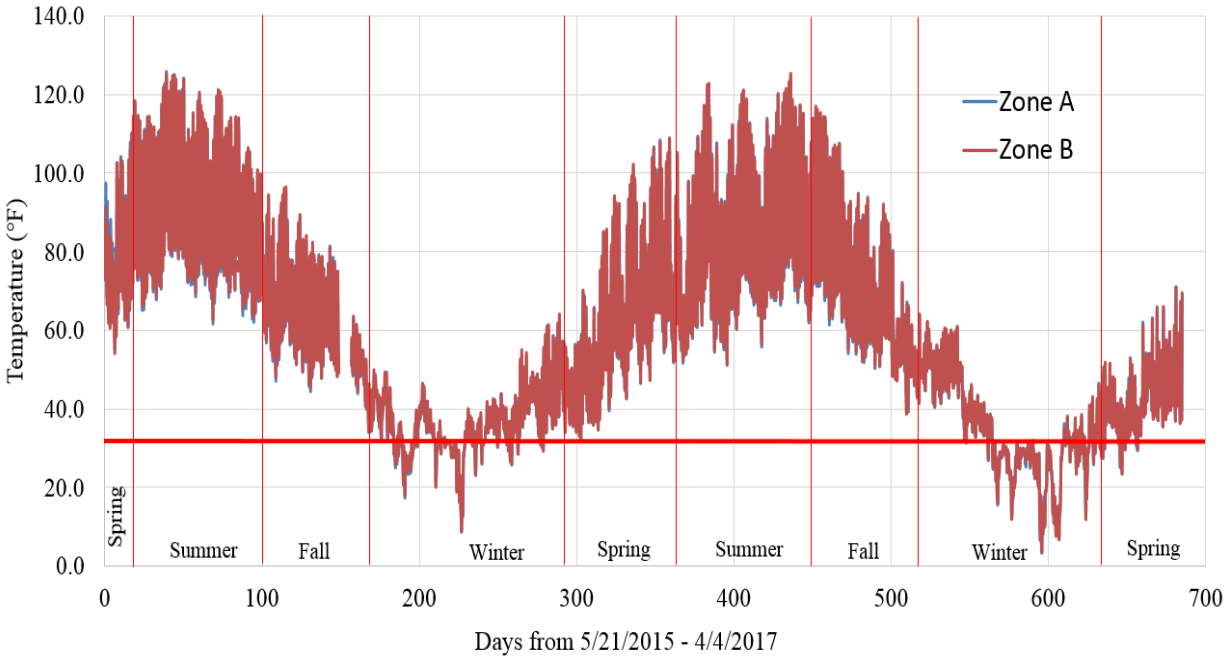

Figure 3.14 PCP temperature from Sensor Tree A and B at 2-inch depth

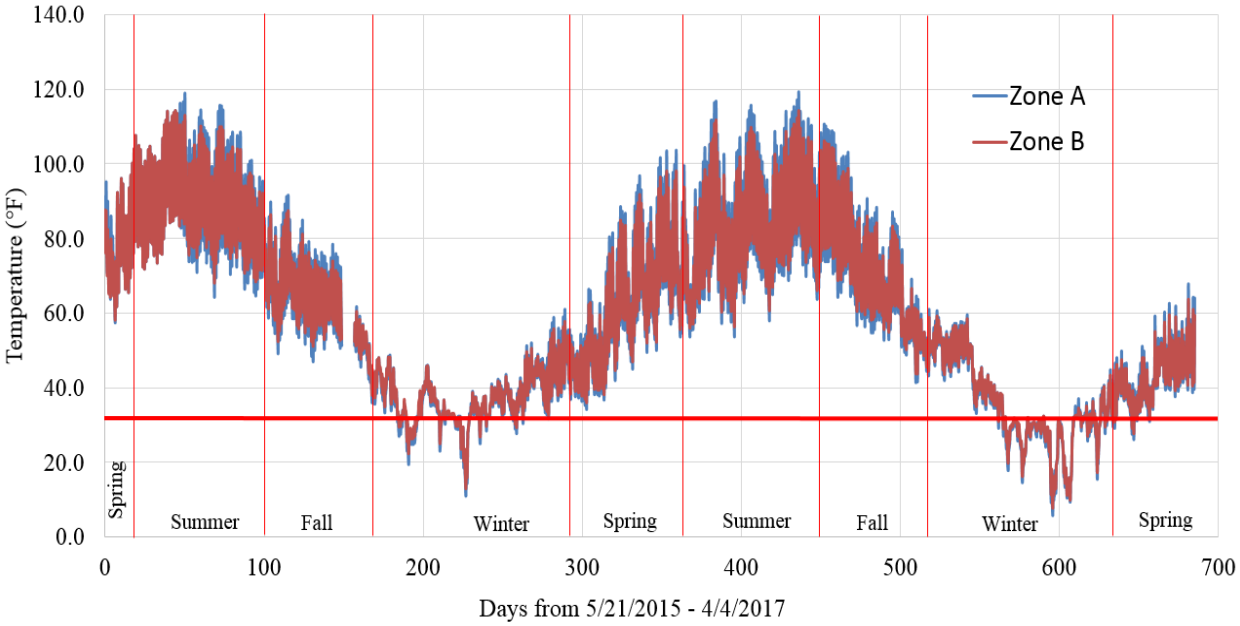

Figure 3.15 PCP temperature from Sensor Tree A and B at 3-inch depth

Figure 3.16 shows the temperature profile of PCP for all seasons at 0.5-, 1.5-, 2-, and 3-inch depth at Zone A from May 21, 2015, to April 4, 2017. Higher temperature fluctuations of PCP at all depths were observed during the summer seasons. The fluctuations decreased

gradually through the fall, becoming minimal during the winter. Higher fluctuations throughout the year were observed for the surface, indicating that the surface has less insulation. Further, the surface had lower temperatures during winter and higher temperatures during spring, implying that freezing and thawing occurred more often at the surface.

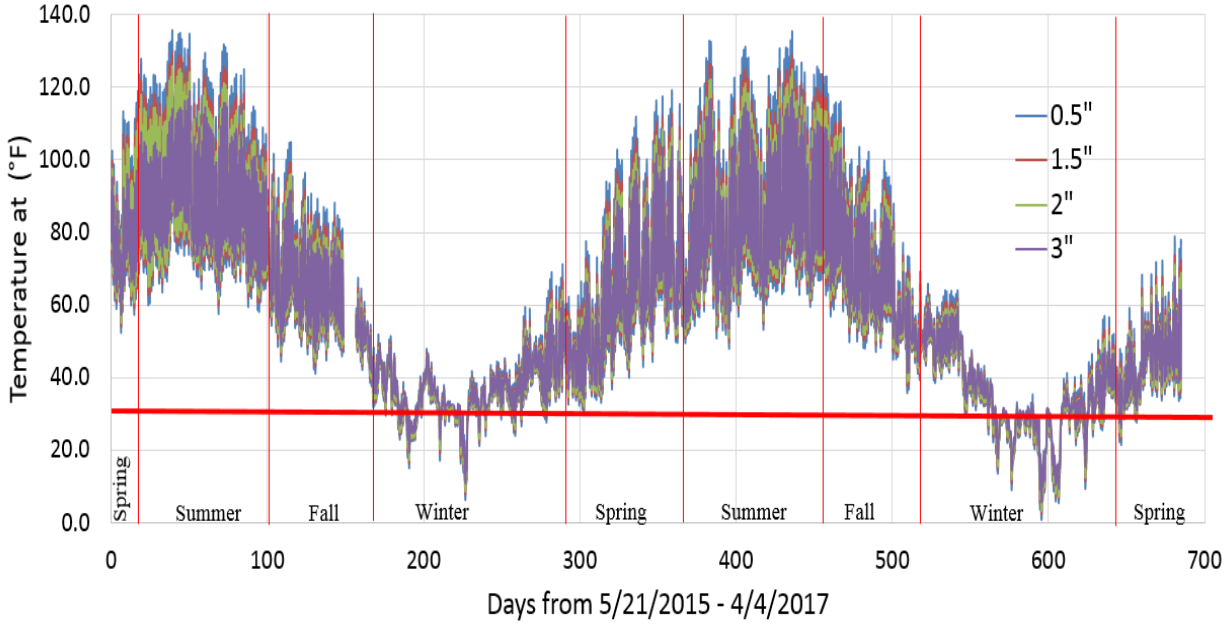

Figure 3.16 Temperature profile of PCP at 0.5-, 1.5-, 2-, and 3-inch depth recorded in Zone **A**

3.4 Winter Temperature Prediction for PCP

The temperature of the PCP was predicted based on ambient conditions during winter. Temperature prediction data were compared against the measured data in the field to evaluate the reliability of the model in predicting the in-field temperature.

3.4.1 Enhanced Integrated Climatic Model

The Enhanced Integrated Climatic Model (EICM), developed by Professor Dempsey at the University of Illinois at Urbana-Champaign, was used in this study to predict the temperature of the PCP section at different depths during the cold weather period from November 2015 through February 2016. The results of temperature prediction obtained from the EICM were

compared with measured temperature data from the field to evaluate the level of accuracy and reliability of the predictions. EICM is a computer model used to predict temperature and moisture content throughout pavement structure with time, based on materials and pavement structural features, provided climatic data, and other environmental information. The EICM uses the finite-difference method (FDM) to solve the heat transfer differential equation with time in one-dimensional space. The heat transfer model implemented in the EICM considers the basic mechanisms of heat transfer, which include conduction, convection, and radiation in the pavement. At the surface, the EICM considers the heat transfer between pavement and the atmosphere in the form of radiation, irradiation, and convection using the thermal properties of the PC layer, also shown schematically in Figure 1.1. Equation 3.2 presents the basic form of the net amount of radiation considered in the EICM (Dempsey et al. 1985).

$$Q_{rad} = Q_s - Q_r - Q_e + Q_a \quad \text{Eq. 3.2}$$

where

Q_s = Radiation from space, Btu/hr· $ft^{2\cdot}$ °F

Q_r = Reflection from clouds, Btu/hr· $ft^{2\cdot}$ °F

Q_e = Reflection from the pavement, Btu/hr· $ft^{2\cdot}$ °F

Q_a = Radiation bounced from clouds. Btu/hr· $ft^{2\cdot}$ °F

The rate of heat transfer by convection between the pavement surface and the air is presented in Equation 3.3 built in to the EICM. Convection is a function of surface convection coefficient, which is a function of wind speed, surface temperature, and ambient temperature (Dempsey et al. 1985).

$$q_c = h_c(T_c - T_a) \quad \text{Eq. 3.3}$$

where

q_c = Convection heat flux, Btu/hr· $ft^{2\cdot}$ °F

h_c = Surface convection coefficient, Btu/hr· $ft^{2\cdot}$ °F

If wind speed (w) ≤ 5, $h_c = 20 + 14w$, else $h_c = [25.6 \cdot 0.78 \cdot w]$

T_c = Concrete surface temperature, °F

T_a = Ambient temperature, °F

3.4.2 EICM Inputs

Climatic Data

The EICM requires hourly environmental inputs of ambient temperature, wind speed, percent sunshine, precipitation, relative humidity, and groundwater table during the analysis period. The meteorological conditions were obtained from the AgWeatherNet weather data source on the WSU – Pullman campus, about 0.5 miles from the site of the instrumented sidewalk. More information regarding the weather station can be found in Nantasai (2016). Hourly groundwater table depths are required as one of the inputs. However, they are not relevant to the pavement temperature prediction since water tables are not encountered during excavation of the subgrade soil. Therefore, an assumption of 15 feet was made.

Q_e and Q_a are calculated internally by the EICM using cloud cover conditions, represented by the hourly percent sunshine input. However, this input was not readily available and needed to be converted from measured on-site solar radiation by using Equation 3.4 (Dempsey et al. 1985).

$$S = \left[\frac{1}{B} \cdot \left(\frac{Q_i}{R^*} - A\right)\right] \cdot 100 \qquad \text{Eq. 3.4}$$

where

S = Percentage of sunshine, which accounts for the influence of cloud cover, %

Q_i = Radiation from the sky ($Q_i = Q_s - Q_r$) in Btu/hr· $ft^{2\cdot}$ °F. Q_i was captured in 15-minute increments with the solar radiation sensor implemented at the project site.

A, B = Constants that account for diffuse scattering and adsorption by the atmosphere. The values of A and B in the Midwest were shown to be 0.0202 and 0.539, respectively; these values did not fluctuate significantly from region to region (Dempsey et al. 1985).

R* = Extraterrestrial radiation (dependent on the latitude of the site and the solar declination of the sun, which is the position of the sun north or south of the equator and is a function of the time of the year).

Extraterrestrial radiation (R*) can be calculated from the solar declination, latitude, zenith angle, and solar constant for a given location (Dempsey et al. 1985). The value of total R* does not change from year to year at any given geographic location. However, it varies parabolically throughout the day, from time of sunrise to time of sunset, while R* is taken as zero during nighttime. R* was obtained by using a code developed in MATLAB based on the formulation for calculating R* in the EICM report. More details regarding this calculation are provided in Nantasai (2016). The values of Q_{rad} and Q_i follow the same behavior as R* (Dempsey et al. 1985).

Structural and Material Properties of PCP Structure

PCP layer

The EICM was originally developed for conventional concrete and asphalt pavements and thereby does not have provisions for PCP. Thus, traditional PCC was selected as the surface layer for the model, with adjustments in the physical properties to better represent the PCP structure. The 6-inch PCP layer was divided into three sublayers equally thick to account for the

vertical density distribution in the pervious concrete layer, which occurs as a result of compaction from the top (Haselbach and Freeman 2006). Note that several preliminary runs of the software revealed that the temperature predictions were not significantly sensitive to the thickness of the sublayers. Figure 3.17 shows a one-dimensional sketch of the PCP system created in the EICM for temperature prediction analysis.

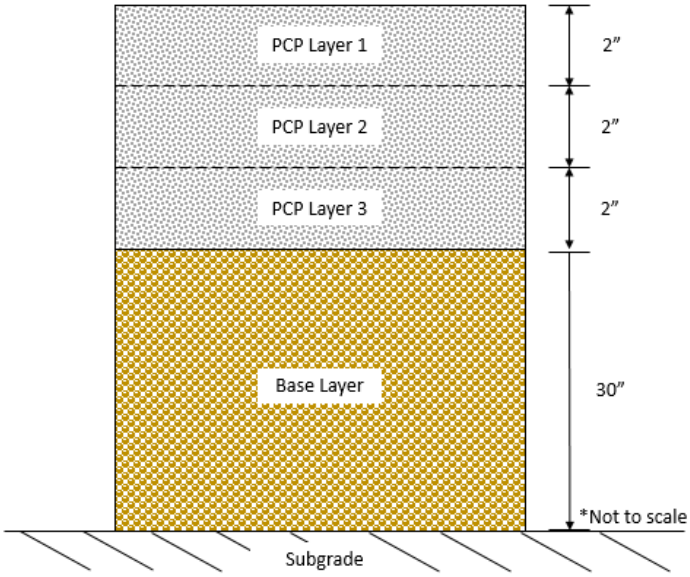

Figure 3.17 Pavement structure created in the EICM for heat transfer analysis

Based on laboratory experiment results discussed previously, a linear correlation of density and porosity can be expressed in Equation 3.5:

$$\rho = -163P + 167.4 \qquad \text{Eq. 3.5}$$

where

ρ = density, lb/ft^3

P = whole porosity, %

The whole porosity of the complete PC layer in the field was not available. Therefore, the relationship between infiltration and porosity developed in another study was used to estimate the slab's *in situ* porosity. The whole porosity of the PC layer was calculated based on the linear

correlation of porosity and infiltration of PCP, as presented in Equation 3.6 (Haselbach et al. 2017).

$$P = 0.002I + 20 \quad \text{Eq. 3.6}$$

where

P = whole porosity, %

I = Infiltration (cm/hr)

Infiltration tests were conducted on the PCP sidewalk at various locations. The infiltration test result of the sensor location, which is 1,570 in/hr (~4,000 cm/hr), was used to calculate the whole porosity. This whole porosity was then used in Equation 3.5 to estimate the slab's density.

Porosity across the depth of the PCP layer varies due to the field compaction method used, with PC being denser at the top, less dense in the middle, and least dense at the bottom. Therefore, the vertical porosity distribution for the PC layer was estimated for the three layers: top, middle, and bottom (Haselbach and Freeman 2006). The 6-inch PCP layer defined in the EICM was divided in three sublayers, as illustrated in Figure 3.17. The vertical distribution of porosity at different sublayer sections was calculated based on Equations 3.7, 3.8, and 3.9 (Haselbach and Freeman 2006). The calculated porosities of the top, middle, and bottom sublayers of the PC layer are provided in

3. These values were entered into the EICM as porosity for PCP at sublayers 1, 2, and 3, respectively and provided the volume faction of air in the mixture.

$$P_{top} = 1.07P - 7 \quad \text{Eq. 3.7}$$

$$P_{mid} = P \quad \text{Eq. 3.8}$$

$$P_{bot} = 0.93P + 7 \quad \text{Eq. 3.9}$$

where

P_{top} = Porosity at top third section of the PCP depth, %

P_{mid} = Porosity at middle third section of the PCP depth, %

P_{bot} = Porosity at middle third section of the PCP depth, %

3 provides a summary of the final physical and thermal properties inputs for the model.

Table 3.3 Summary of inputs for the EICM evaluations

Pavement Layer	Calculated Porosity	Density (lb/cu ft)	Thickness (inch)	Thermal Properties k (Btu/ft^2 ·h ·˚F) Cp (Btu/lb ·˚F)	
PCP Layer 1	0.23	130	2	k	0.32
				Cp	0.22
PCP Layer 2	0.28	124	2	k	0.27
				Cp	0.22
PCP Layer 3	0.32	118	2	k	0.23
				Cp	0.22
Base Layer	0.35	130	30	k	0.30
				Cp	0.20
Subgrade Layer	0.30	118	200	k	0.80
				Cp	0.22

The volumetric fractions of the aggregate and paste constituents were obtained based on the mixture design. The thermal conductivity of PCP made with limestone was computed using the volume fractions obtained from mixture proportioning in Table 2.2 and using the model presented in Equation 3.1 to simulate *k* of the PCP sidewalk. For heat capacity, the parallel model in Equation 1.2 was used. Typical values of specific heat of aggregate, paste, and air were found in the literature and are listed in Table 3.4.

Table 3.4 Thermal property of each constituent of the PCP

Constituent	Cp (Btu/lb ˚F)	Reference

Limestone Aggregate	0.29	Goranson (1942)
Cement Paste	0.20	Fu (1997)
Air void	0.024	Cengel et al. (2008)

Properties of the sublayers

The 30-inch base and subgrade layers were defined as coarse aggregate and silt-clay soil, classified as A-1-a and A-4, respectively (AASHTO M 145-91 2012). The values of porosity and density of the base and subgrade were left as the program defaults, which are 35% and 130 lb/ft^3 for the base layer and 30% and 118 lb/ft^3 for the subgrade layer. In addition, the default values were used for their thermal properties, as shown in

.

Temperature predictions at selected depths of pavement are calculated based on the corresponding nodes assigned in the EICM, which were set to match the locations of the sensors installed in the PCP in the field to compare and evaluate the accuracy of the temperature predictions at corresponding depths.

Initial temperature inputs

The EICM requires input of initial temperature for each layer at assigned nodes. The initial temperature values are used for the first iteration in the FDM and, therefore, influence the accuracy of the predictions for the initial time increments. The actual values of temperature of the PCP in the field at each depth at the start of the analysis period (November 1, 2015, at midnight) were used as the initial temperature for each node. The solar absorptivity of 0.8 was used for the PCP surface, which is the default value of solar absorptivity of PCC in the EICM.

3.4.3 EICM Temperature Predictions

In this section, the temperature prediction for PCP during the winter season is discussed. The comparison of field temperature profiles in Zones A and B discussed previously indicated that the measured temperature of PCP in the two zones is relatively similar. Therefore, the predicted temperatures for PCP were only compared with the temperature data measured in Zone A. Figure 3.18 shows the EICM temperature predictions at 0.5-, 1.5-, 2-, and 3-inch depth. Figure 3.19 through Figure 3.22 show the EICM temperature predictions in comparison with the corresponding measured temperature in Zone A at 0.5-, 1.5-, 2-, and 3-inch depth. The red horizontal line in the figures indicates the temperature at 32°F.

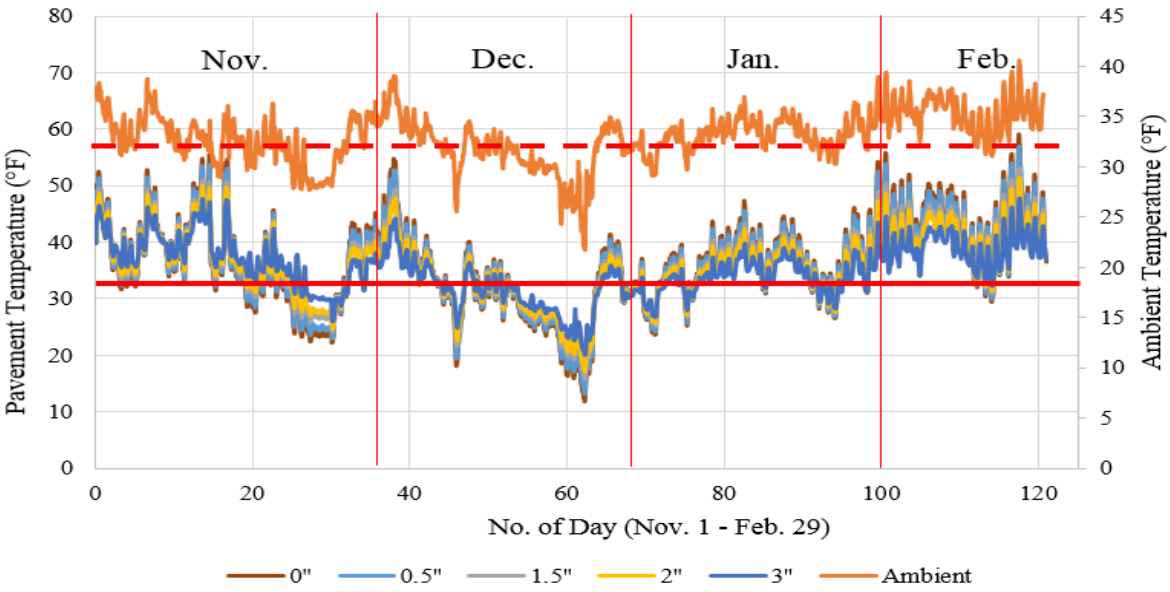

Figure 3.18 EICM temperature predictions for PCP at 0.5-, 1.5-, 2-, and 3-inch depths

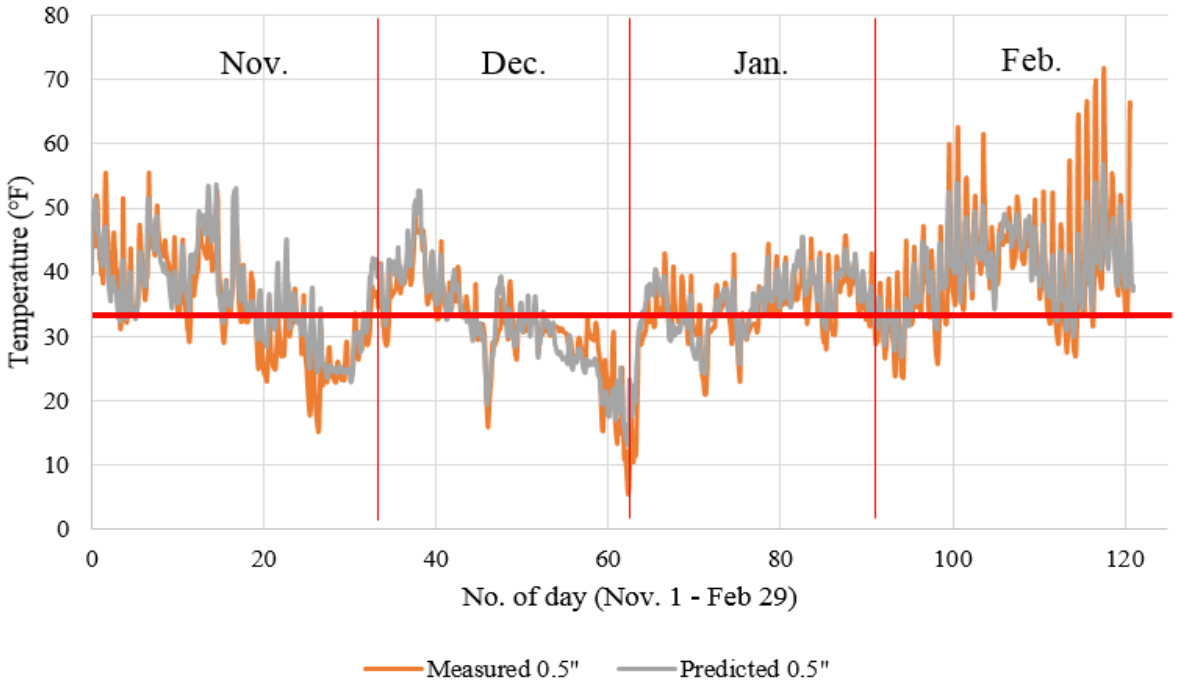

Figure 3.19 Comparison of predicted and measured temperatures of PCP at 0.5-inch depth

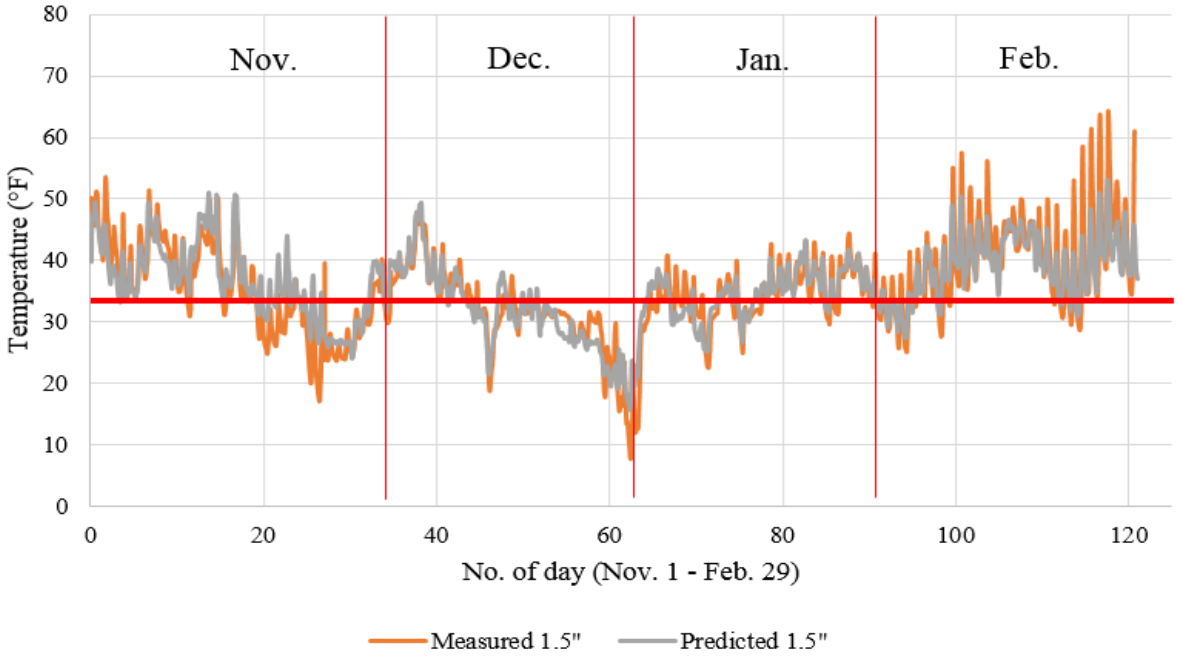

Figure 3.20 Comparison of predicted and measured temperatures of PCP at 1.5-inch depth

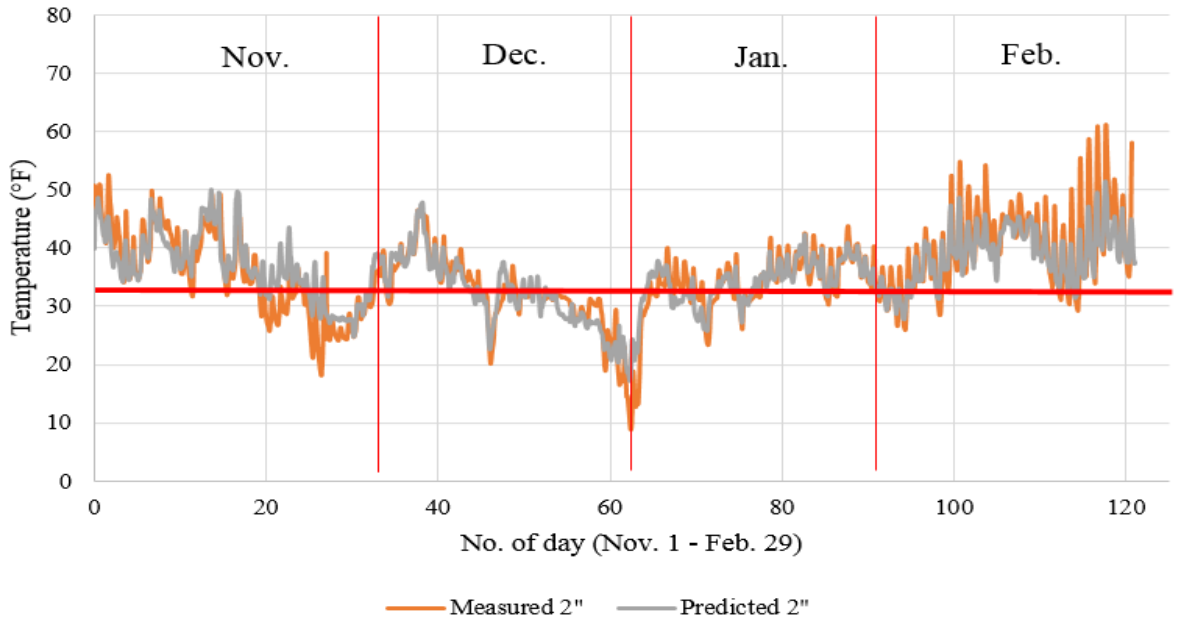

Figure 3.21 Comparison of predicted and measured temperatures of PCP at 2-inch depth

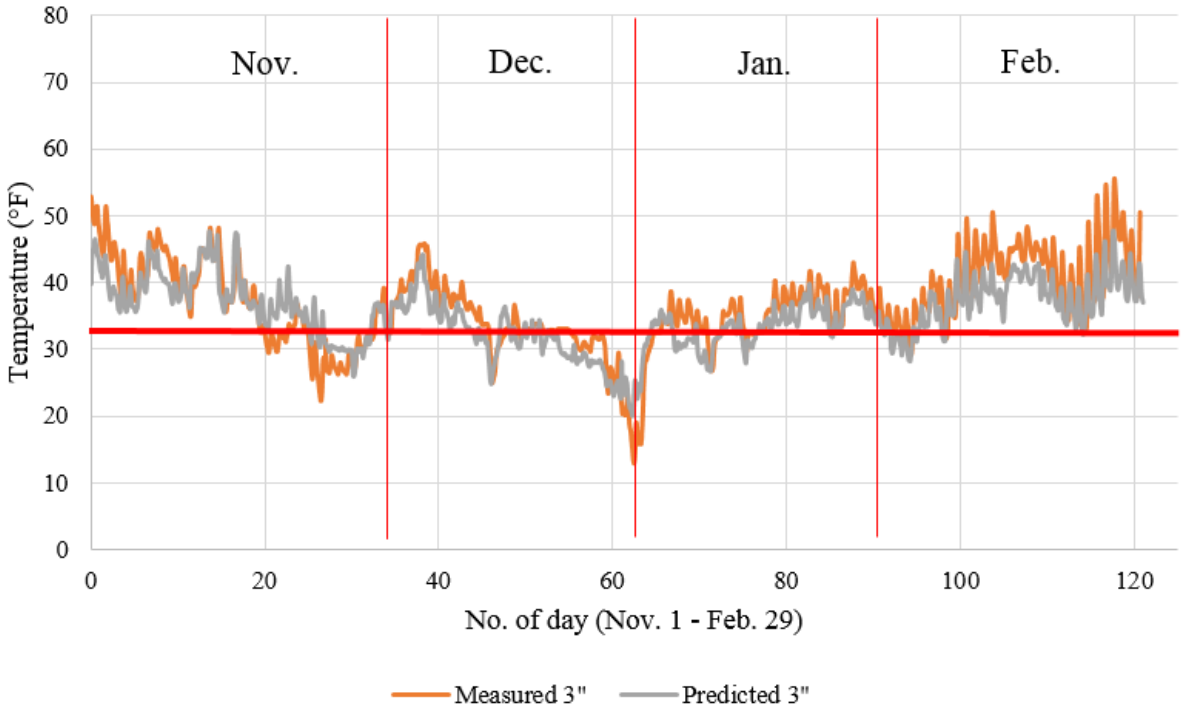

Figure 3.22 Comparison of predicted and measured temperatures of PCP at 3-inch depth

Discussion of EICM Temperature Prediction Results

Slight variations between the predicted and the measured temperature for all depths were observed throughout the winter season. Figure 3.19 through Figure 3.22 show that the EICM temperature prediction of PCP at all depths is exceptionally accurate during November 2015 through the end of January 2016, where the error between the predicted and the measured temperature averaged to approximately 5°F, and the maximum temperature difference is approximately 10°F. Starting in February 2016, the measured temperature, especially at the surface of the PCP sidewalk, shows larger daily fluctuations than the predicted temperature. The average error of the EICM temperature prediction in February is approximately 11°F. The maximum difference between the measured and the predicted temperature during February is 14.9, 12.3, 10.2, and 7.8°F for pavement depths of 0.5, 1.5, 2, and 3 inches, respectively. This fluctuation may be caused by pavement exposure to higher solar radiation during February than during November through January, as represented in Figure 2.9 (Nantasai 2016). The PCP absorbs solar energy, which may then be given off as heat (Kevern et al. 2012). The fluctuation may also be caused by the solar absorptivity value used in the EICM, which is a built-in value for conventional PCC (Nantasai 2016). More accurate values for solar absorptivity of PCP have not yet been established. The surface layer of PCP is less insulated than the lower layers, causing it to have a higher temperature fluctuation. As shown in Figure 3.20 through Figure 3.22, moving down through the layers, the temperature fluctuation decreases due to higher insulation.

As mentioned previously, the EICM was designed to analyze the effects of climate on rigid and flexible pavements. The rigid (PCC) pavement structure option was selected for the model created in EICM. Adjustment of density, porosity, and thermal properties were made to simulate the properties of PCP. The variation between the predicted and the measured

temperature at 3-inch depth might be due to moisture in the bottom layer. Moisture could have been trapped inside the PCP during the winter season and was unable to evaporate, thus causing higher *k* than the *k* input in the EICM. Overall, the EICM model is capable of predicting the PCP surface temperature within 3°F on average during wintertime. Table 3.3 shows the coefficient of determination (R^2) and the standard error of the estimate (SEE) for temperature predictions at different depths with respect to measured temperature in the field.

Table 3.3 Statistical report of EICM temperature predictions with respect to measured temperature of PCP at different depths.

Depth	Coefficient of Determination (R^2)	Standard Error of the Estimate (SEE)
0.5"	0.75	1.24
1.5"	0.71	3.36
2.0"	0.66	3.31
3.0"	0.51	3.64

3.4.4 Regression Model for Surface Temperature Prediction

To identify the freezing potential of the PCP surface, the days that the PCP surface fell below 32°F were identified. Out of the 121-day analysis period, the number of days that the temperature of the PCP at a depth 0.5 inch dropped below 32°F was 67 days based on measured data, and 57 days based on the predicted temperature. Therefore, the EICM model for the sidewalk is able to identify that the PCP surface temperature dropped below 32°F for 85% of the days. These are the days that PCP has the potential to freeze, especially when exposed to moisture. The data show that the ambient temperature was equivalent or below 32°F for 63 days out of the 121-day analysis period, implying that other environmental factors affect the pavement surface temperature.

For practical purposes, it is beneficial to develop an easy-to-use statistical model that can be used to predict when deicers should be applied to PCP. Since the temperature of the top

portion of the PCP is mainly influenced by meteorological parameters, it was used in the statistical model.

A multiple regression analysis was conducted in Minitab to predict the surface temperature as a function of ambient conditions including temperature, relative humidity, wind speed, and solar radiation. The results of the regression analysis are provided in Equation 3.10. The *p*-value of the regression is less than 0.001 at 98% confidence interval with a mean standard error of 0.2°F and R^2 of 0.98. The maximum level of accuracy of this equation is achieved when used to predict the temperature of PCP at the surface for the PCP sidewalk at the project location because its materials, porosities, and location are sensitive. This equation can be used as an estimation of the PCP surface temperature for other pavements. However, depending on the PC mixture design and the structural features of the PCP, this equation may not result in a high level of accuracy.

$$PCP\ surface\ temperature = 15.28 + 0.3486 \cdot T_{amb} + 0.1152 \cdot h_c + 0.03 \cdot S - 108.6 \cdot P - 0.0458 \cdot RH + 0.006350 \cdot T_{amb}^2 - 0.004546 \cdot h_c^2 + 0.005284 \cdot T_{amb} \cdot h_c - 0.000869 \cdot T_{amb} \cdot S + 0.001159 \cdot T_{amb} \cdot RH + 0.001394 \cdot h_c \cdot S - 0.000199 \cdot S \cdot RH + 1.211 \cdot P \cdot RH \quad \text{Eq. 3.10}$$

where

T_{amb} = Ambient temperature, °F

h_c = Wind speed, mph

S = Percent sunshine, %

P = Precipitation, in

RH = Relative humidity, %

CHAPTER 4. CONCLUSIONS AND RECOMMENDATIONS

Conclusions

Deicers are applied on pavement surfaces for ice and snow control, to provide sufficient surface friction, and to prevent slipping accidents. The best outcome is obtained through a timely application of deicers. This project investigated the thermal properties and heat transfer mechanism of PCP to predict the pavement temperature for enhancement of winter maintenance operations. Temperature predictions were compared with pavement temperature data measured in the field to evaluate the level of prediction reliability.

Two methodologies were used to measure thermal conductivity (*k*): heat flow using a heat flow meter and heat impulse using a thermal sensor probe. Two types of specimens were cast and tested for the experiment: 4-inch cylinders and slabs. The *k* of PC was tested in both dry and wet conditions. Thermal conductivity was evaluated against the porosity of PC. Strong linear relationships were found between porosity and density as well as porosity and *k*. Thermal conductivity of PC varies with the physical properties (density/porosity) of the PC structure. The PC tested using the heat flow machine resulted in lower values of *k* than when tested using the thermal sensor probe. One explanation may be that the sensor probe can only capture the *k* of the top 2 inches of PC specimens.

A linear relationship was developed between *k* and porosity. The *k* of PC is higher in wet conditions than in dry conditions by approximately 30%.

Temperature sensors were installed inside a PCP sidewalk at the Washington State University – Pullman campus to capture temperature at different depths throughout the thickness of the pavement over time. A solar radiation sensor was also implemented at the project site to capture radiation from the sky, accounting for net radiation on cloudy days. Ambient conditions

were monitored throughout time and evaluated side-by-side with the measured pavement temperature. The measured temperature profile during the winter season was compared with the pavement prediction model.

Temperature predictions for PCP were explored to enhance winter maintenance operations by making suggestions on appropriate days to apply deicers based on ambient conditions. Enhanced Integrated Climatic Model (EICM) computer software was used to predict the temperature of PCP throughout depth based on ambient variables, including ambient temperature, wind speed, radiation of the sky, relative humidity, and precipitation. The thermal and physical properties of PCP established in this study were used as input parameters for the EICM software. The EICM temperature prediction data were compared with field measured temperature data.

Although the temperature prediction provided by the EICM had slightly lower fluctuations than the measured temperature of PCP, the prediction of the top 3 inches of PCP closely followed the trend of measured temperature. The magnitude of fluctuation decreases with the depth of the pavement due to increases in insulation of the PCP structure. Solar radiation has a high influence on the EICM temperature model prediction.

Overall EICM predictions for days when the PCP temperature fell below 32˚F agreed with the field observations 85% of the time.

A regression model was suggested using climatic indices to predict the PCP surface temperature. The regression model is sensitive to materials, porosity, and location, but it can be used as an estimation of temperature prediction at the PCP surface.

Recommendations for Future Work

More PC specimens in different mixture designs and aggregate types at different porosities should be tested for thermal conductivity to add to the database developed in this study. More research should be conducted for testing the *k* of PC at a lower temperature range for cold-climate conditions. Research on thermal properties of the base layer and thermal conduction between the PCP and base layer may minimize the variations between predicted and measured temperature at lower levels of the PCP and help improve the level of accuracy. The regression model can be further expanded to include thermophysical properties and layer thickness as variables for wider applications.

References

AASHTO M 145-91 (2012). *Standard Specification for Classification of Soils and Soil-Aggregate Mixtures for Highway Construction Purposes.* American Association of State and Highway Transportation Officials.

ACI (2010). ACI Committee 522, American Concrete Institute & International Organization for Standardization. *Report on Pervious Concrete (ACI 522R-10).*

Ashley, E. (2008). "Using pervious concrete to achieve LEED points." Concrete in Focus. <http://www.perviouspavement.org/downloads/LEED_PointsAshley.pdf> (2015).

ASTM International. (2009). *ASTM C1701/C1701M-09 Standard Test Method for Infiltration Rate of In Place Pervious Concrete*. Retrieved from https://doi.org/10.1520/C1701_C1701M-09

ASTM International. (2012). *ASTM C1754/C1754M-12 Standard Test Method for Density and Void Content of Hardened Pervious Concrete*. Retrieved from https://doi.org/10.1520/C1754_C1754M-12

ASTM International. (2015). *ASTM C518-15 Standard Test Method for Steady-State Thermal Transmission Properties by Means of the Heat Flow Meter Apparatus*. Retrieved from https://doi.org/10.1520/C0518-15

ASTM International. (2016). *ASTM C192/C192M-16a Standard Practice for Making and Curing Concrete Test Specimens in the Laboratory*. Retrieved from https://doi.org/10.1520/C0192_C0192M-16A

Boyer, M. (2011). *Preliminary Analysis of Summertime Heat Storage in Traditional Versus Pervious Concrete Systems.* (Doctoral dissertation, Washington State University.)

Cengel, Y. A., Turner, R. H., Cimbala, J. M., and Kanoglu, M. (2008). *Fundamentals of Thermal-Fluid Sciences*. New York, NY: McGraw-Hill.

Chopra, M., Wanielista, M., Spence, J., Ballock, C., and Offenberg, M. (2006). "Hydraulic Performance of Pervious Concrete Pavements." *Proc., 2006 Concrete Technology Forum*.

Cook, R. D. (2007). *Concepts and Applications of Finite Element Analysis*. John Wiley & Sons.

Delatte, N., Miller, D., and Mrkajic, A. (2007). *Portland cement pervious concrete pavement: Field performance investigation on parking lot and roadway pavements.* Ready Mixed Concrete (RMC) Research and Education Foundation.

Dempsey, B. J., Herlache, W. A., and Patel, A. J. (1985). *Environmental Effects on Pavements: Theory Manual*. U.S. Department of Transportation, Federal Highway Administration.

EPA. (2002). *Source Water Protection Practices Bulletin–Managing Highway Deicing to Prevent Contamination of Drinking Water. EPA 816-F-02-019.* U.S. Environmental Protection Agency.

Eppelbaum, L., Kutasov, I., and Pilchin, A. *Applied Geothermics.* SpringerLink, doi: 10.1007/978-3-642-34023-9, 2014.

Flower, W., Burian, S. J., Pomeroy, C. A., and Pardyjak, E. R. (2010). "Surface Temperature and Heat Exchange Differences between Pervious Concrete and Traditional Concrete and Asphalt Pavements." In *Low Impact Development 2010: Redefining Water in the City*, 1417-1430.

Fricke, B. A. (1992). *Soil Thermal Conductivity: Effects of Saturation and Dry Density. (Doctoral dissertation, University of Missouri-Kansas City.)*

Fu, X., and Chung, D.D.L. (1997). "Effects of silica fume, latex, methylcellulose, and carbon fibers on the thermal conductivity and specific heat of cement paste." *Cement and Concrete Research,* 27(12), 1799-1804.

Goranson, R. W. (1942). "Heat capacity; heat of fusion." *Geological Society of America Special Papers*, 36, 223-242.

Gui, J., Phelan, P. E., Kaloush, K. E., and Golden, J. S. (2007). "Impact of pavement thermophysical properties on surface temperatures." *Journal of Materials in Civil Engineering*, 19(8), 683-690.

Harmathy, T. Z. (1970). "Thermal properties of concrete at elevated temperatures." *Journal of Materials*.

Haselbach, L., and Freeman, R. (2006). "Vertical porosity distributions in pervious concrete pavement." *ACI Materials Journal,* 103(6), 452-458.

Haselbach, L., Boyer, M., Kevern, J., and Schaefer, V. (2011). "Cyclic heat island impacts on traditional versus pervious concrete pavement systems." *Transportation Research Record: Journal of the Transportation Research Board,* (2240), 107-115.

Haselbach, L., Werner, B., Dutra, V. P., Schwetz, P., da Silva Filho, L. P., Batezini, R., and Balbo, J. T. (2017). Estimating Porosity of In Situ Pervious Concrete Using Surface Infiltration Tests. *Journal of Testing and Evaluation*, *45*(5).

Hu, J., Wang, K., and Ge, Z. (2009, August). "Study of Iowa PCC thermal properties for mechanistic-empirical pavement design." *Proc., the 2009 Mid-Continent Transportation Research Symposium,* Ames, Iowa.

Kevern, J. T., and Schaefer, V. R. (2008). "Temperature response in a pervious concrete system designed for stormwater treatment." In *GeoCongress 2008: Geosustainability and Geohazard Mitigation*, 1137-1144.

Kevern, J. T., and Schaefer, V. R. (2013). "Mixture proportioning considerations for improved freeze-thaw durability of pervious concrete." In *ISCORD 2013: Planning for Sustainable Cold Regions*, 471-481.

Kevern, J. T., Wang, K., and Schaefer, V. R. (2009 a). "Effect of coarse aggregate on the freeze-thaw durability of pervious concrete." *Journal of Materials in Civil Engineering*, 22(5), 469-475.

Kevern, J., Schaefer, V., and Wang, K. (2009 b). "Temperature behavior of pervious concrete systems." *Transportation Research Record: Journal of the Transportation Research Board*, 2098, 94-101.

Kevern, J. T., Haselbach, L., and Schaefer, V. R. (2012). "Hot weather comparative heat balances in pervious concrete and impervious concrete pavement systems." *Journal of Heat Island Institute International*, 7(2).

Kim, K. H., Jeon, S. E., Kim, J. K., and Yang, S. (2003). "An experimental study on thermal conductivity of concrete." *Cement and Concrete Research*, 33(3), 363-371.

Kosmatka, S. H., Panarese, W. C., and Kerkhoff, B. (2002). *Design and control of concrete mixtures.* Vol. 5420, pp. 60077-1083. Skokie, IL: Portland Cement Association.

Lamond, J. and Pielert, J. (2006), Eds. *Significance of Tests and Properties of Concrete and Concrete-Making Materials*, STP169D-EB, ASTM International, West Conshohocken, PA, https://doi.org/10.1520/STP169D-EB

Larson, G., and Dempsey, B. J. (1997). *Enhanced Integrated Climatic Model, Version 2.0*. Department of Civil and Environmental Engineering.

Nantasai, B. (2016). *Temperature Predictions in Pervious Concrete Pavement during Cold Months.* (Master's dissertation, Washington State University.)

Nassiri, S. (2011). *Establishing Permanent Curl/Warp Temperature Gradient in Jointed Plain Concrete Pavements,* (Doctoral dissertation, University of Pittsburgh.)

Nassiri, S. and Nantasai, B. (2017). "Thermal conductivity of pervious concrete for various porosities." *ACI Materials Journal*, 114(2).

Obla, K. H., and Sabnis, G. (2009). *Pervious Concrete for Sustainable Development*. Boca Raton, FL.

PCA. (2015, July). (Portland Cement Association). "Freeze-Thaw Resistance." Concrete Technology, <http://www.cement.org/Learn/concrete-technology/durability/freeze-thaw-resistance>

Robertson, E. C. (1988). *Thermal properties of rocks. (No. 88-441).* U.S. Geological Survey.

Schaefer, V., Kevern, J., Izevbekhai, B., Wang, K., Cutler, H., and Wiegand, P. (2010). "Construction and performance of pervious concrete overlay at Minnesota Road Research Project." *Transportation Research Record: Journal of the Transportation Research Board,* 2164, 82-88.

Shu, X., Huang, B., Wu, H., Dong, Q., and Burdette, E. G. (2011). "Performance comparison of laboratory and field produced pervious concrete mixtures." *Construction and Building Materials,* 25(8), 3187-3192.

Tong, B. (2011). *Clogging Effects of Portland Cement Pervious Concrete.* (Master Thesis, Iowa State University.)

Ye, D. (2007). *Early-age Concrete Temperature and Moisture Relative to Curing Effectiveness and Projected Effects on Selected Aspects of Slab Behavior.* (Doctoral dissertation, Texas A&M University.)

Zhang, R., Jiang, G., and Liang, J. (2015). "The albedo of pervious cement concrete linearly decreases with porosity." *Advances in Materials Science and Engineering*.